haematologica
Journal of the Ferrata Storti Foundation

# Targeting CD19-positive lymphomas with the antibody-drug conjugate loncastuximab tesirine: preclinical evidence as single agent and in combination therapy

by Chiara Tarantelli, David Wald, Nicolas Munz, Filippo Spriano, Alessio Bruscaggin, Eleonora Cannas, Luciano Cascione, Eugenio Gaudio, Alberto J. Arribas, Shivaprasad Manjappa, Gaetanina Golino, Lorenzo Scalise, Maria Teresa Cacciapuoti, Emanuele Zucca, Anastasios Stathis, Giorgio Inghirami, Patrick H. Van Berkel, Davide Rossi, Paolo F. Caimi, Francesca Zammarchi, and Francesco Bertoni

*Received: August 29, 2023.*
*Accepted: May 2, 2024.*

*Citation: Chiara Tarantelli, David Wald, Nicolas Munz, Filippo Spriano, Alessio Bruscaggin, Eleonora Cannas, Luciano Cascione, Eugenio Gaudio, Alberto J. Arribas, Shivaprasad Manjappa, Gaetanina Golino, Lorenzo Scalise, Maria Teresa Cacciapuoti, Emanuele Zucca, Anastasios Stathis, Giorgio Inghirami, Patrick H. Van Berkel, Davide Rossi, Paolo F. Caimi, Francesca Zammarchi, and Francesco Bertoni. Targeting CD19-positive lymphomas with the antibody-drug conjugate loncastuximab tesirine: preclinical evidence as single agent and in combination therapy. Haematologica. 2024 May 9. doi: 10.3324/haematol.2023.284197 [Epub ahead of print]*

**Targeting CD19-positive lymphomas with the antibody-drug conjugate loncastuximab tesirine: preclinical evidence as single agent and in combination therapy**

Chiara Tarantelli* [1^], David Wald [2^], Nicolas Munz [1], Filippo Spriano [1], Alessio Bruscaggin [1], Eleonora Cannas [1], Luciano Cascione [1,3], Eugenio Gaudio [1], Alberto J. Arribas [1,3], Shivaprasad Manjappa [4], Gaetanina Golino [1], Lorenzo Scalise [1], Maria Teresa Cacciapuoti [5], Emanuele Zucca [1,6], Anastasios Stathis [6,7], Giorgio Inghirami [5], Patrick H. van Berkel [8], Davide Rossi [1,6], Paolo F. Caimi [9], Francesca Zammarchi [8], Francesco Bertoni* [1,6]

[1] *Institute of Oncology Research, Faculty of Biomedical Sciences, USI, Bellinzona, Switzerland;*
[2] *Case Western Reserve University, Cleveland, OH, USA;*
[3] *SIB Swiss Institute of Bioinformatics, Lausanne, Switzerland;*
[4] *Fred Hutchinson Cancer Center, Seattle, Washington, USA;*
[5] *Department of Pathology and Laboratory Medicine, Weill Cornell Medicine, New York, NY;*
[6] *Oncology Institute of Southern Switzerland, Ente Ospedaliero Cantonale, Bellinzona, Switzerland;*
[7] *Faculty of Biomedical Sciences, USI, Lugano, Switzerland;*
[8] *ADC Therapeutics (UK) Ltd., London, UK;*
[9] *Cleveland Clinic/Case Comprehensive Cancer Center, Cleveland, OH, USA.*

^, first co-authors

*Co-corresponding authors:
-Dr Chiara Tarantelli, Institute of Oncology Research, via Francesco Chiesa 5, 6500 Bellinzona, Switzerland. Phone: +41 58 666 7202; e-mail: chiara.tarantelli@ior.usi.ch

-Prof. Francesco Bertoni, Institute of Oncology Research, via Francesco Chiesa 5, 6500 Bellinzona, Switzerland. Phone: +41 58 666 7206; e-mail: francesco.bertoni@ior.usi.ch

**Fundings**
This project was partially supported by research funds from ADC Therapeutics, the Swiss National Science Foundation grant SNSF 310030_197466, the Swiss Cancer Research grant KFS-4713-02-2019 (to FB), LLS 7027-23, LLS-SCOR 7026-21 (GI). NM was supported by a Ph.D. Fellowship of the NCCR RNA & Disease, a National Centre of Competence in Research funded by the Swiss National Science Foundation (grant numbers 182880, 205601).

**Acknowledgments**
We thank our Colleagues Dr Antonella Zucchetto and Dr Valter Gattei (Aviano, Italy) for their helpful discussion.

**Data sharing**
All data are included in the manuscript and in the supplementary material.

**Author Contributions**
CT: performed experiments, data mining, interpreted data and co-wrote the manuscript.
FS, EG: performed experiments and interpreted data.
LC: performed data mining.
DW, EC, AJA, GG, LS, MTC, GI: performed experiments.
NM, AB: performed experiments and data mining.
AB, DR: performed targeted DNA sequencing and data mining.

EZ, AS: provided advice.

PHVB, FZ: co-designed the study, provided reagents, and supervised the study.

FB: co-designed the study, performed data mining, interpreted data, supervised the study, and co-wrote the manuscript.

All authors reviewed and accepted the final version of the manuscript.

**Conflict of interests**

CT: travel grant from iOnctura. LC: travel grant from HTG Molecular Diagnostics. EZ: advisory boards of BeiGene, BMS, Curis, Eli/Lilly, Incyte, Janssen, Merck, Miltenyi Biomedicine, and Roche; received research support from AstraZeneca, Beigene, BMS/Celgene, Incyte, Janssen, and Roche, received a travel grant from BeiGene, Janssen, Gilead, and Roche. AS: advisory boards from Janssen, Roche; research funding from AbbVie, ADC Therapeutics, Amgen, AstraZeneca, Bayer, Cellestia, Incyte, LoxoOncology, Merck MSD, Novartis, Pfizer, Philogen, Roche; travel grant from AstraZeneca. Expert testimonies from Bayer, Eli Lilly. DR: honoraria from AstraZeneca, AbbVie, BeiGene, BMS/Celgene, Janssen; research funding from AstraZeneca, AbbVie, BeiGene, Janssen. PHVB, FZ: ADC Therapeutics: employment and stocks ownership. PFC: research funding from ADC Therapeutics and grants from Genentech; advisory board consultancy fee from ADC Therapeutics, Novartis, BMS, Genentech, and SOBI. FB: institutional research funds from ADC Therapeutics, Bayer AG, BeiGene, Helsinn, HTG Molecular Diagnostics, Ideogen AG, Idorsia Pharmaceuticals Ltd., Immagene, ImmunoGen, Menarini Ricerche, Nordic Nanovector ASA, Oncternal Therapeutics, Spexis AG; consultancy fee from BIMINI Biotech, Helsinn, Menarini; advisory board fees to institution from Novartis; expert statements provided to HTG Molecular Diagnostics; travel grants from Amgen, Astra Zeneca, iOnctura. The other Authors have no conflicts of interest.

**Abstract**

Antibody-drug conjugates (ADCs) represent one of the most successful therapeutic approaches introduced in clinical practice in the last few years. Loncastuximab tesirine (ADCT-402) is a CD19 targeting ADC, in which the antibody is conjugated through a protease cleavable dipeptide linker to a pyrrolobenzodiazepine (PBD) dimer warhead (SG3199). Based on the results of a phase 2 study, loncastuximab tesirine was recently approved for adult patients with relapsed/refractory large B-cell lymphoma.

We assessed the activity of loncastuximab tesirine using *in vitro* and *in vivo* models of lymphomas, correlated its activity with CD19 expression levels, and identified combination partners providing synergy with loncastuximab tesirine.

Loncastuximab tesirine was tested across 60 lymphoma cell lines. Loncastuximab tesirine had strong cytotoxic activity in B-cell lymphoma cell lines. The *in vitro* activity was correlated with CD19 expression level and intrinsic sensitivity of cell lines to the ADC's warhead. Loncastuximab tesirine was more potent than other anti-CD19 ADCs (coltuximab ravtansine, huB4-DGN462), albeit the pattern of activity across cell lines was correlated. Loncastuximab tesirine activity was also largely correlated with cell line sensitivity to R-CHOP. Combinatorial *in vitro* and *in vivo* experiments identified the benefit of adding loncastuximab tesirine to other agents, especially BCL2 and PI3K inhibitors.

Our data support the further development of loncastuximab tesirine as a single agent and in combination for patients affected by mature B-cell neoplasms. The results also highlight the importance of CD19 expression and the existence of lymphoma populations characterized by resistance to multiple therapies.

## Introduction

Despite the recent improvements, current therapies are not yet curative for too many patients affected by lymphoid neoplasms (1-3), and novel therapeutic strategies are still needed. Antibody-drug conjugates (ADCs) represent one of the most successful therapeutic approaches introduced in clinical practice in the last 25 years (4, 5). ADCs are complex compounds that contain three components: an antibody, a warhead (i.e., a cytotoxic agent), and a linker that joins the two together. ADCs enable targeted delivery of potent warheads into tumor cells using antibodies against tumor antigens.

Due to its pattern of expression and its biological role in lymphocytes, the B cell marker CD19 has been heavily exploited for antibody-based therapies, including ADCs, and, more recently, for cellular therapies (4, 6-10). Loncastuximab tesirine (ADCT-402) is a CD19 targeting ADC, in which the CD19-specific antibody is stochastically conjugated through a protease cleavable dipeptide linker to a pyrrolobenzodiazepine (PBD) dimer warhead (SG3199) (11). Following binding to CD19 positive cells, loncastuximab tesirine is rapidly internalized and transported to lysosomes, where the linker is cleaved to release the PBD dimer SG3199 (11). In contrast with the microtubule-disrupting monomethyl auristatin E (MMAE) used in the CD30-targeting brentuximab vedotin and the CD79B-targeting polatuzumab vedotin ADCs (12, 13), SG3199 belongs to a new generation of DNA cross-linking agents. SG3199 binds to guanine residues in the DNA minor groove, forming covalent cross-links of the two DNA strands (14, 15). Loncastuximab tesirine has been studied in various clinical trials (16-18) and, based on the results of a phase 2 study (16, 19), it was recently approved in the USA and Europe for adult patients with relapsed/refractory (R/R) large B-cell lymphoma after at least two prior lines of systemic therapy (20).

Here, we assessed the anti-tumor activity of loncastuximab tesirine in a large panel of lymphoma cell lines, with a focus on the expression of its target and the identification of active combination partners.

## Methods

Cell lines, and compounds

Full methods are provided in Supplementary Materials and Methods.

*In vitro* cytotoxic activity

The cytotoxic activity of loncastuximab tesirine was assessed *in vitro,* as previously described (21). Briefly, cells were exposed to each compound for 96 hours and assayed by MTT [3-(4,5-dimethylthiazolyl-2)-2, 5-diphenyltetrazoliumbromide]. For R-CHOP treatment, cells were exposed for 72 h to 1 µg/mL CHOP + 100 µg/mL rituximab to five different concentrations in serial dilution 1:10. Rituximab was diluted to clinically recommended serum levels (22) and CHOP represented a mix reflecting the clinical ratios of the drugs (23, 24) (85%, 4-hydroperoxy-cyclophosphamide; 5.5%, doxorubicin; 0.16%, vincristine; 11.1%, prednisolone). Cells were also exposed in parallel to the PBD dimer SG3199 and the isotype-control ADC B12-SG3249 (25).

Synergism assessment was done by exposing cells (96 hours) to increasing doses of loncastuximab tesirine and each of the other agents, either alone or in combination, followed by an MTT assay. Determination of the Chou-Talalay combination index (CI) was done as previously described (26). Combinations were defined as synergistic (median CTI < 0.9), additive (median CTI, 0-9-1.1), or of no benefit/antagonist (median CTI > 1.1).

CD19 expression

Absolute cell surface CD19 expression was determined via quantification of the antigen on the surface of lymphoma cell lines using Quantum Simply Cellular (QSC) anti-Human IgG beads (Bangs Laboratories) to create a calibration curve. Antibody Binding Capacity (ABC) values were then normalized to the control isotype antibody B12.

CD19 RNA expression values were extracted from the datasets GSE94669, previously obtained using a targeted RNA-seq approach (HTG EdgeSeq Oncology Biomarker panel) and a microarray-based technology (Illumina HT-12 arrays) (26) and GSE221770, previously produced via total-RNA-Seq (27).

Patient-derived xenograft (PDX) cell line

Full methods are provided in Supplementary Materials and Methods. PDX was produced in the context of protocols approved by the Cornell University (IRB: 107004999, 0201005295 and 1410015560; Universal consent: 1302013582; *in vivo* protocol 2014-0024).

LyV4.0 CAPP-seq gDNA Assay and variant calling

Full methods are provided in Supplementary Materials and Methods.

Immunoblotting, and cell cycle

Full methods are provided in Supplementary Materials and Methods.

Data mining

Full methods are provided in Supplementary Materials and Methods.

*In vivo* experiments

Full methods are provided in Supplementary Materials and Methods. Mice maintenance and animal experiments were performed under the institutional guidelines established for the Animal Facility at The Institute of Research in Biomedicine (IRB) (license n. TI 49-2018) (TMD8 experiment) or following the policies and regulations set forth by the Institutional Animal Care and Use Committee of Case Western Reserve University (JEKO1 experiment).

**Results**

Loncastuximab tesirine has strong cytotoxic activity in B-cell lymphoma cell lines.

Loncastuximab tesirine was tested for its anti-proliferative activity across 60 lymphoma cell lines, which were exposed to the ADC for 96 hours (Table S2). Loncastuximab tesirine had activity in the picomolar range, with a median $IC_{50}$ of 4.1 pM (95% C.I, 2-9.6 pM), among 48 lymphoma cell lines derived from mature B cell lymphomas. Conversely, the anti-proliferative activity of loncastuximab tesirine was over 800-fold lower in nine T cell lymphoma cell lines (median $IC_{50}$ 3.5 nM; 95% C.I, 0.8-11 nM; $P<0.0001$) (Figure S1). The activity was similar among all the individual B cell lymphoma subtypes except Hodgkin lymphoma models, which were over 600-fold less sensitive to loncastuximab tesirine than the other cell lines ($P=0.009$) (Table 1). Loncastuximab tesirine exerted its anti-lymphoma activity via induction of apoptosis, as shown in two exemplar cell lines derived from ABC (TMD8) or GCB (VAL) DLBCL (Figure S2).

The sensitivity to loncastuximab tesirine did not differ between DLBCL cell lines with (n=15) and without (n=11) *BCL2* translocation or with (n=16) and without (n=7) *TP53* inactivation. Instead, DLBCL cell lines with *MYC* translocation (n=10) versus cell lines without the translocation (n=16) and DLBCL cell lines with (n=7) versus those without (n=19) concomitant *BCL2* and *MYC* translocation (double hit) had lower $IC_{50}$ values (both comparisons, $P<0.05$) (Figure S3).

The sensitivity to loncastuximab tesirine was also correlated with mutational status obtained from a targeted DNA sequencing designed to cover various coding genomic regions recurrently mutated in mature B-cell neoplasms (Table S4). After multiple corrections, no somatic mutation was significantly associated with the loncastuximab tesirine response.

In parallel, we exposed the cells to an isotype-control ADC (B12-SG3249), which was active in the nanomolar range with no difference between B and T cell lymphoma cell lines: median $IC_{50}$ values were 0.9 nM (95% C.I, 0.7-2.2 nM) and 1.7 nM (95% C.I, 0.8-12 nM), respectively.

Finally, loncastuximab tesirine was tested in three non-human lymphoma cell lines: $IC_{50}$ values were 2 nM and 500 pM in two mouse cell lines and 175 pM in a canine DLBCL cell line, similar to what was achieved using the isotype-control ADC B12-SG3249, indicating a non-cross species anti-lymphoma activity not driven by CD19 targeting (Table S2).

CD19 levels correlate with loncastuximab tesirine cytotoxic activity

We then focused on cell lines derived from mature B cell lymphomas to assess whether CD19 cell surface expression levels correlated with the anti-tumor activity of loncastuximab tesirine. We measured the absolute CD19 surface expression levels on each cell line (Table S2), and we used additional protein and RNA expression data we had previously obtained on the same panel of cell lines (27, 28). We observed that the CD19 expression levels associated with loncastuximab tesirine

activity, as demonstrated by the negative correlation between $IC_{50}$ values and CD19 expression values measured both at the cell surface protein level [(absolute quantitation, n=46, r=-0.44, P=0.002; relative quantitation, n=45, r=-0.4, P=0.006]) and RNA level [(microarrays, n=53, r=-0.74, P<0.0001; HTG, n=36, r=-0.5 P=0.002; RNA-Seq, n=44, r=-0.55, P<0.0001] (Figure 1A-E).
Based on the association mentioned above between the presence of *MYC* translocation and loncastuximab tesirine lower $IC_{50}$ values (i.e., higher sensitivity), we explored the possible relationships between CD19 and MYC expression levels in DLBCL cells. Neither CD19 surface protein expression levels nor CD19 RNA levels differed between cell lines with or without MYC translocation (single genetic event or together with BCL2 translocation) (Figure S4A-C). Similarly, CD19 and MYC levels were not correlated (Figure S4D-E). Finally, MYC RNA levels were negatively correlated with loncastuximab tesirine $IC_{50}$ values (R=-0.35) but without reaching a statistical significance (P=0.089) (Figure S4F).

The cytotoxic activity of loncastuximab tesirine's warhead SG3199 is not affected by the lymphoma subtype but differs based on the presence of genetic lesions.
All cell lines were exposed to loncastuximab tesirine's warhead SG3199 (Table S2). The median $IC_{50}$ value was 0.85 pM (95% C.I, 0.69-1.14) across all 60 lymphoma cell lines. Differently from what was observed with loncastuximab tesirine, the activity of SG3199 did not differ between B and T cell lymphomas (Table 2, Figure S5), and there was no correlation between the SG3199 $IC_{50}$ values and CD19 expression values (Figure S6). SG3199 was more potent than the ADC. The difference in terms of $IC_{50}$ values between SG3199 and loncastuximab tesirine was statistically significant both considering all cell lines (P<0.0001) or cell lines derived from B cell lymphomas (P<0.0001) (Figure S7).
The sensitivity to SG3199 appeared reduced in DLBCL cell lines with *TP53* inactivation when compared to *TP53* wt cell lines (P<0.001) (Figure S8A). The *BCL2* translocation *per se* did not affect the sensitivity to SG3199 (Figure S8B). Like what was observed with loncastuximab tesirine, SG3199 was more active in DLBCL bearing *MYC* translocation as a single event or concomitant with *BCL2* translocation (P<0.05) (Figure S8C-D). No correlation was observed between sensitivity to SG3199 and MYC RNA levels (Figure S9).

The cytotoxic activities of loncastuximab tesirine and its warhead SG3199 are highly correlated.
The cytotoxic activity of loncastuximab tesirine and its warhead were highly positively correlated among all the cell lines (r=0.60, P<0.0001) and within the cell lines derived from mature B cell lymphomas (r=0.63, P<0.0001) (Figure 2). Most of the cell lines that were less sensitive to the ADC ($IC_{50}$ values higher than the $75^{th}$ percentile, i.e., 768 pM) but sensitive to SG3199 ($IC_{50}$ values lower than the $75^{th}$ percentile, i.e., 2.9 pM) were represented by the CD19 negative models (T cell lymphomas, HL) and the non-human lymphomas. Some cell lines, such as the splenic MZL VL51, were highly sensitive to the warhead, but due to low CD19 expression, high loncastuximab tesirine $IC_{50}$ (VL51 $IC_{50}$ >100 fold the median B cell lymphoma cell lines $IC_{50}$). There were a few cell lines, especially the mantle cell lymphoma (MCL) REC1 and the DLBCL Pfeiffer and U2932, which had $IC_{50}$ values higher than the $75^{th}$ percentile for both loncastuximab tesirine and SG3199 warhead, suggestive of a primary resistance to the warhead. The GCB DLBCL cell line SU-DHL-6 was sensitive to loncastuximab tesirine but resistant to its warhead SG3199. We confirmed that the anti-tumor activity was driven by the activity of the antibody itself rather than by the antibody complexed to the toxin (Figure S10).

The cytotoxic activity of loncastuximab tesirine is correlated with the cytotoxicity of other CD19-targeting ADCs
We exploited data previously produced in our laboratory on the same panel of cell lines with two CD19 targeting ADCs, coltuximab ravtansine (SAR3419), comprising the maytansinoid microtubule disruptor DM4, and huB4-DGN462, incorporating a DNA-alkylating payload (28). The pattern of activity of loncastuximab tesirine correlated with both coltuximab ravtansine (r=0.38, P=0.01) and

huB4-DGN462 (r=0.6, P<0.0001) (Figure S11). Loncastuximab tesirine was more potent than both huB4-DGN462 (P=0.034) and coltuximab ravtansine (P<0.0001), although the exposure time previously used for the two additional ADCs was shorter (72 vs 96 hours). REC1, Pfeiffer, and U2932, the cell lines most resistant to loncastuximab tesirine, were also resistant to huB4-DGN462 and coltuximab ravtansine.

The pattern of cytotoxic activity of loncastuximab tesirine and R-CHOP are correlated.

We exposed DLBCL cell lines (n=26) to the *in vitro* equivalent of R-CHOP (rituximab, cyclophosphamide, doxorubicin, vincristine, and prednisone) (Table S3). The $IC_{50}$ values obtained with R-CHOP correlated with the $IC_{50}$ values of both loncastuximab tesirine (r=0.655, P<0.001) and SG3199 (r=0.425, P=0.03) (Figure 3). Some cell lines presented a reduced sensitivity to R-CHOP ($IC_{50}$ values higher than the 75$^{th}$ percentile, i.e., 0.077 µg/mL) but were very sensitive to loncastuximab tesirine and its warhead. A few cell lines (Pfeiffer, U2932, SU-DHL-16, SU-DHL-2) were less sensitive to loncastuximab tesirine and R-CHOP.

Loncastuximab tesirine is active in post-CART lymphoma cells.

We took advantage of PDX-derived cells from a patient treated with CART19 therapy (SS POST CAR19) to investigate a novel potential clinical application of loncastuximab tesirine. Cells expressed surface CD19 at a 26.72-fold level normalized to isotype (Figure S14). Loncastuximab tesirine showed anti-proliferative activity ($IC_{50}$=0.7 nM), superior to the naked antibody rB4v1.2 and to the isotype associated with toxin B12-C220-SG3249 ($IC_{50}$ values of 17.8 nM and not reached because $IC_{50}$ was beyond the tested range, respectively). The sensitivity to loncastuximab tesirine was below the 75$^{th}$ percentile in cell lines. Cells were still sensitive to the toxin ($IC_{50}$=0.37 pM).

Loncastuximab tesirine-based combinations appear beneficial *in vitro*

We explored the potential benefit of combining loncastuximab tesirine with drugs having an established role in treating lymphoma patients. We tested these combinations in two GCB DLBCL cell lines (VAL and WSU-DLCL2), two ABC DLBCL (TMD8 and OCI-LY-3) and two MCL (JEKO1 and JVM2). The combination partners were the BCL2 inhibitor venetoclax, the PI3Kδ inhibitor idelalisib, the PIK3α/δ inhibitor copanlisib, the anti-CD20 monoclonal antibody rituximab, the chemotherapy agent bendamustine, and the PARP inhibitor olaparib (Table 3). The combinations of loncastuximab tesirine with the proteasome inhibitor bortezomib, the BTK inhibitor ibrutinib, and the immunomodulator lenalidomide, were only tested the ABC DLBCL cell lines, as these drugs are only used for the treatment of ABC DLBCL.

In DLBCL, the most beneficial combinations were loncastuximab tesirine plus venetoclax or idelalisib, with synergism achieved in all the models tested, followed by the ADC plus bendamustine, copanlisib or olaparib. Synergism was also observed in one (OCI-Ly-3) of the two ABC DLBCL cell lines tested with loncastuximab tesirine plus ibrutinib. Combination with rituximab was synergistic in one cell line (VAL). No advantage was seen in combining loncastuximab tesirine with bortezomib or lenalidomide. In MCL, the most beneficial combinations were observed with venetoclax and copanlisib, with synergism in two out of two cell lines. The addition of idelalisib was synergistic in only one cell line (JVM2).

The effect on cell cycle was investigated in four DLBCL cell lines (TMD8, OCI-LY-3, VAL, and WSU-DLCL2) treated with loncastuximab tesirine and the most promising targeted agents, i.e., venetoclax, idelalisib and copanlisib, as single agents and in combination, after 96 hours of treatments. In all the DLBCL cell lines, the increase in sub-G1, compatible with cell death, was higher than in control in loncastuximab tesirine-treated cells either as a single agent or in combination (Figure S12). Treatments with venetoclax, idelalisib, and copanlisib as single agents also increased sub-G1 in WSU-DLCL2 and VAL and OCI-LY-3. In TMD8, an increase in sub-G1 was observed only in a single copanlisib treatment.

To understand the mechanism sustaining the benefit given by loncastuximab tesirine when combined with venetoclax, idelalisib, or copanlisib, specific signaling pathways were explored by immunoblotting

in TMD8 (ABC DLBCL) and WSU-DLCL2 (GCB DLBCL) cell lines (Figure 4, Figure S13). CD19 downregulation was observed in both cell lines following treatment with loncastuximab tesirine alone after 24 hours of treatment, and the downregulation increased further when loncastuximab tesirine was combined with each of the three drugs. The levels of pAKT were reduced in cells treated with the PI3K inhibitors idelalisib and copanlisib as single agents or in combination with loncastuximab tesirine (Figure 4, Figure S13). The levels of the anti-apoptotic protein MCL1 were downregulated by treatment with loncastuximab tesirine in the TMD8 cell line, and the effect was maintained in the combinations. In the WSU-DLCL2 cell line, MCL1 levels were also down-regulated in cells treated with loncastuximab tesirine and with the PI3K inhibitors as single agents and in combination. In both cell lines, exposure to venetoclax upregulated MCL1, which was reduced in combination with loncastuximab tesirine. Cleaved PARP1, a marker of apoptosis, was slightly increased when loncastuximab tesirine was combined with the other three drugs.

Loncastuximab tesirine-based combinations are beneficial *in vivo*

An ABC DLBCL xenograft (TMD8 cell line) was used to validate the combination of loncastuximab tesirine with copanlisib *in vivo*. We first evaluated both compounds as single agents to define the doses to be combined. Mice (n.= 5 per group) bearing subcutaneously (sc) TMD8 xenografts were treated with control (PBS, iv), three different doses of loncastuximab tesirine (0.1 mg/Kg vs. 0.3 mg/Kg vs. 0.6 mg/Kg; iv qd x 1), two different doses of the non-binding control ADC B12-SG3249 (0.3 mg/Kg vs 0.6 mg/Kg; iv qd x 1) (Figure S15), or two different schedules of copanlisib (13 mg/Kg, iv; 1 day on/6 days off vs two days on/5 days off) (Figure S16). We defined the sub-active schedules of the drugs used in the combination study based on the observed dose-dependent anti-tumor activity for both loncastuximab tesirine and copanlisib. Thus, the combination experiment included animals treated with a single dose of loncastuximab tesirine (0.3 mg/Kg iv; day 1; n.=7) or copanlisib (13 mg/kg iv, one day on/6 days off; day 1, 8; n.=7) as single agents or in combination (n.=9) (Figure 5A). As a control, a group of mice was treated with vehicle (PBS) or non-binding control ADC B12-SG3249 at 0.3 mg/kg (n.=4 each, iv, qd x 1; day 1). The combination of loncastuximab tesirine with the PIK3$\alpha$/$\delta$ inhibitor copanlisib decreased tumor volume compared to vehicle, isotype control and single treatments (Area Under the Curve, AUC, combination=1.115; vehicle=3.702; B12-SG3249=2.883; copanlisib=1,952; loncastuximab tesirine=2,032). After day 1, the anti-tumor effect of the combination was always superior to the copanlisib ($q<0.001$), loncastuximab tesirine ($q<0.001$), vehicle ($q<0.001$), and ADC isotype control ($q<0.001$) treatment. The anti-tumor activity of B12-SG3249 did not differ from vehicle alone ($q>0.1$) or versus the other single agent treatments. In terms of tumor weight, the effect of the combination was superior to the single agents ($p=0.003$; combo vs. copanlisib, $p<0.0001$; combo vs loncastuximab tesirine, $p<0.0001$; combo vs ADC isotype, $p=0.003$) (Figure S17A). The combination presented an additive/slight synergistic coefficient of drug interaction (CDI) at day 38 (CDI=0.959 using B12-SG3249 as control; CDI=1.03 using merged vehicle and B12GS3249 as control). No toxicities were observed with single agents or combinations in this setting.

A MCL xenograft model (JeKo1) was used to assess the combination of loncastuximab tesirine with venetoclax. Mice (n=4 per group) were treated with a single injection of loncastuximab tesirine (1 mg/kg iv) and/or venetoclax (100mg/kg PO daily five days a week) or vehicle at day 16 after cell injection when all tumors were palpable. Tumor volume was decreased in the combination arm compared to vehicle and single treatments (AUC, combination=2,059; vehicle=4,692; venetoclax=3,470; loncastuximab tesirine=4,162), and the anti-tumor effect was statistically significant compared to the vehicle and loncastuximab tesirine ($q<0.001$) as a single agent at all time points but day1 (Figure 5B, Figure S17B). A synergistic coefficient of drug interaction (CDI=0.53) was calculated for this combination at the end of the experiment (day 15).

**Discussion**

Here, we have shown that i) the CD19 targeting ADC loncastuximab tesirine has a strong cytotoxic activity in a large panel of cell lines derived from B cell lymphomas, ii) its *in vitro* activity correlated with CD19 expression level, and iii) there is benefit of adding loncastuximab tesirine to other agents,

especially BCL2 and PI3K inhibitors. We also showed the similarities and differences in activity with its warhead, other CD19-targeting ADCs, and R-CHOP.

These findings extend the initial preclinical data (11), confirming loncastuximab tesirine cytotoxic activity in mature B cell lymphomas. In the initial publication, only a weak trend was observed between the anti-tumor activity of loncastuximab tesirine and CD19 expression levels across ten cell lines, including CD19-negative cells (11). Here, we expanded the number of cell lines analyzed, and even when focusing on B cell lymphoma models only, we observed a significant correlation between the activity of loncastuximab tesirine and CD19 expression on cell surface as well as CD19 RNA levels, using multiple platforms, including one specifically designed for the analysis of formalin-fixed paraffin-embedded clinical specimens (29). So far, immunohistochemistry (IHC) performed on tumor samples from the loncastuximab tesirine phase 1 and the phase 2 trials have not demonstrated a correlation between CD19 expression and ORR, with patients with extremely low or no detectable CD19 IHC expression responding to loncastuximab tesirine (17, 30). However, our data in cell lines and the observation that measuring the CD19 surface density in addition to the IHC expression improves the response prediction (30) suggest that more sensitive measurements of CD19 in clinical specimens might be helpful to predict the type and the duration of response of patients treated with loncastuximab tesirine.

Besides loncastuximab tesirine, we tested its warhead, SG3199, on all the cell lines. As expected, SG3199 did not correlate with CD19 expression, and it was equally active in CD19-positive and CD19-negative cell lines. Interestingly, the anti-tumor activity of loncastuximab tesirine correlated with the intrinsic sensitivity of the cell lines to SG3199. Indeed, we could identify three different groups of cell lines. One group of cell lines was highly sensitive to loncastuximab tesirine and SG3199 and presented the highest CD19 expression. A second group of cell lines was sensitive to the warhead but not to the ADC ($IC_{50}$ values higher than the $75^{th}$ percentile). These included models not derived from human B cell lymphomas but also from B cell lymphomas with low CD19 expression. One example was the VL51 cell line, derived from splenic MZL. Interestingly, we recently reported that VL51 derivatives with resistance to PI3K and BTK inhibitors, acquired after months of exposure to idelalisib or ibrutinib, present higher CD19 expression levels than the parental cells and an increased sensitivity to loncastuximab tesirine (31) and anti-CD19 chimeric antigen receptor (CAR) T cells (32), further indicating the importance of CD19 expression levels. A third group of cell lines was characterized by $IC_{50}$ values of SG3199 and loncastuximab tesirine higher than the $75^{th}$ percentiles, indicative of low sensitivity to the agents and intrinsic resistance to the PBD warhead.

There was no effect of histology, DLBCL cell of origin*, TP53* or *BCL2* genes status on the *in vitro* cytotoxic activity of loncastuximab tesirine. Among DLBCL cell line models, we discovered an association between *MYC* translocation, as a single event or together with BCL2 translocation, and a higher sensitivity to loncastuximab tesirine and its warhead, which might be sustained by the interplay between MYC-induced replication stress and the SG3199-induced DNA interstrand cross-links (33-35). The clinical relevance of this finding remains to be determined. Interestingly, in the phase 2 study, cases with *MYC* translocation were as sensitive as the remaining patients. This suggests that even this group of otherwise poor-outcome patients can benefit from the ADC (36).

The cytotoxic activity of PBD dimers can occur via TP53-independent and TP53-dependent mechanisms (34), and we observed a decreased activity of SG3199 in *TP53*-inactive DLBCL cell lines when compared with the wt *TP53* models. Although this difference was not observed when cells were exposed to loncastuximab tesirine, it suggests that payloads with an alternative mechanism of action might work better in the context of an inactive TP53.

Next, we compared the activity of loncastuximab tesirine against all cell lines with the activity of R-CHOP, which is used in the first-line treatment of DLBCL. Loncastuximab tesirine was more active in many cell lines with low/moderate sensitivity to R-CHOP. Still, the anti-tumor activity of loncastuximab tesirine and its warhead significantly correlated with the activity of R-CHOP. Indeed, there were cell lines that were very sensitive to all treatments and, conversely, cell lines with resistance to R-CHOP and loncastuximab tesirine and its warhead.

We took advantage of a previous study (28) and we compared the activity of loncastuximab tesirine to coltuximab ravtansine and huB4-DGN462, two other CD19 targeting ADCs which were analyzed using the same panel of cell lines. Interestingly, despite a higher potency, the cytotoxic activity of loncastuximab tesirine correlated with both coltuximab ravtansine and huB4-DGN462. The correlation was higher with the latter ADC, which is *in vitro* and *in vivo* more potent than coltuximab ravtansine (28), and carries the DNA-alkylating agent indolinobenzodiazepine pseudodimer DGN462 as warhead (28), rather than the maytansinoid microtubule disruptor N2′-deacetyl-N2′-(4-mercapto-4-methyl-1-oxopentyl) (DM4 or ravtansine) (37), present in coltuximab ravtansine. This observation and the comparison with R-CHOP highlight the importance of finding novel treatment modalities, including new active molecules as payloads.

We combined loncastuximab tesirine with other anti-lymphoma agents to identify potentially active combinations that may provide better patient outcomes. In DLBCL, the loncastuximab tesirine-based combinations that were synergistic in most cell lines included those with the BCL2 inhibitor venetoclax, PI3K inhibitors (idelalisib, copanlisib), and with chemotherapy agent bendamustine, followed at less extent by the PARP inhibitor olaparib, the BTK inhibitor ibrutinib and the anti-CD20 monoclonal antibody rituximab. The *in vitro* findings with venetoclax and the PI3K inhibitors were extended to MCL cell lines and confirmed *in vivo*. While venetoclax has been extensively combined with small molecules, much less data regarding the combination with ADCs is available. Synergy with venetoclax has been previously reported for two ADCs bearing microtubule targeting agents as payloads, the CD79B targeting polatuzumab vedotin and the CD205 targeting MEN1309. Exposure to both agents, containing MMAE and DM4, respectively, caused down-regulation of MCL1 (38, 39) due to protein degradation via the ubiquitin/proteasome system (38). Also, alkylating agents have been shown to induce proteasome-mediated degradation of MCL1 (40); hence, we anticipate a similar mechanism of action mediated by loncastuximab tesirine via its SG3199 payload and sustaining the observed synergism with venetoclax. The combination of loncastuximab tesirine and venetoclax is currently being explored in a phase 1 study (NCT05053659). No trial is being conducted to examine the combination of loncastuximab tesirine with PI3K inhibitors, which appears promising based on the *in vitro* and *in vivo* anti-tumor activity. The novel highly specific PI3Kδ inhibitors seem to have an improved toxicity profile (41, 42), which might overcome the problems observed with first-generation compounds (43).

The combination of loncastuximab tesirine with ibrutinib, supported by other preclinical work (44), has been clinically evaluated with results reported in R/R DLBCL or MCL (45). The toxicity was manageable, and the overall response rates were 67% in non-GCB DLBCL, 20% in GCB DLBCL, and 86% in MCL (45).

The benefit of combining loncastuximab tesirine with a PARP inhibitor could lead to novel clinical opportunities. The observed benefit of combining a PBD-based ADC with a PARP inhibitor aligns with the data reported mainly in BRCA-deficient solid tumor models (46-48). Interestingly, the GCB DLBCL marker LMO2 inhibits BRCA1 recruitment to DNA double-strand break in DLBCL cells, causing a BRCA1-deficiency-like phenotype and sensitizing DLBCL cells to PARP inhibition (49). Indeed, we observed synergism in the GCB DLBCL cells but only an additive effect in one of the two ABC DLBCL models. PARP inhibitors have been explored in lymphoma patients (50). In particular, the PARP inhibitor veliparib has shown evidence of clinical activity, including complete remissions and safety in combination with bendamustine plus or minus rituximab (50, 51).

Since multiple CD19-targeting therapeutic modalities are available that share CD19 loss as one of the mechanisms of resistance (4, 6-10, 52), it will be crucial to define the best sequencing or prioritization strategy for using these agents (53-57), as well as their integration with bispecific antibodies (6-8). Here, we demonstrated the *in vitro* activity of loncastuximab tesirine in a cell line derived from a patient progressing after CD19-targeting chimeric antigen receptor (CAR) T-cell therapy, strengthening the clinical data showing responses in patients after CAR-T cells (53, 57).

In conclusion, our data support the further development of loncastuximab tesirine as a single agent and in combination for patients affected by mature B cell neoplasms. The results also highlight the

importance of CD19 expression and the existence of lymphoma populations characterized by resistance to multiple therapies.

**References**

1. Roser M, Ritchie H. Cancer. 2019. Available from: https://ourworldindata.org/cancer, accessed on November 1st 2023.

2. Sung H, Ferlay J, Siegel RL, et al. Global Cancer Statistics 2020: GLOBOCAN Estimates of Incidence and Mortality Worldwide for 36 Cancers in 185 Countries. CA Cancer J Clin. 2021;71(3):209-249.

3. Sehn LH, Salles G. Diffuse Large B-Cell Lymphoma. N Engl J Med. 2021;384(9):842-858.

4. Barreca M, Lang N, Tarantelli C, Spriano F, Barraja P, Bertoni F. Antibody-drug conjugates for lymphoma patients: preclinical and clinical evidences. Explor Target Antitumor Ther. 2022;3(6):763-794.

5. Dumontet C, Reichert JM, Senter PD, Lambert JM, Beck A. Antibody-drug conjugates come of age in oncology. Nat Rev Drug Discov. 2023;22(8):641-661.

6. Abramson JS, Ghosh N, Smith SM. ADCs, BiTEs, CARs, and Small Molecules: A New Era of Targeted Therapy in Non-Hodgkin Lymphoma. Am Soc Clin Oncol Educ Book. 2020;40:302-313.

7. de Ramon Ortiz C, Wang S, Stathis A, et al. How to integrate CD19 specific chimeric antigen receptor T cells with other CD19 targeting agents in diffuse large B-cell lymphoma? Hematol Oncol. 2024;42(1):e3237.

8. Sermer D, Elavalakanar P, Abramson JS, Palomba ML, Salles G, Arnason J. Targeting CD19 for diffuse large B cell lymphoma in the era of CARs: Other modes of transportation. Blood Rev. 2023;57:101002.

9. Bailly S, Cartron G, Chaganti S, et al. Targeting CD19 in diffuse large B-cell lymphoma: An expert opinion paper. Hematol Oncol. 2022;40(4):505-517.

10. Varma G, Goldstein J, Advani RH. Novel agents in relapsed/refractory diffuse large B-cell lymphoma. Hematol Oncol. 2023;41 Suppl 1:92-106.

11. Zammarchi F, Corbett S, Adams L, et al. ADCT-402, a PBD dimer-containing antibody drug conjugate targeting CD19-expressing malignancies. Blood. 2018;131(10):1094-1105.

12. Francisco JA, Cerveny CG, Meyer DL, et al. cAC10-vcMMAE, an anti-CD30-monomethyl auristatin E conjugate with potent and selective antitumor activity. Blood. 2003;102(4):1458-1465.

13. Dornan D, Bennett F, Chen Y, et al. Therapeutic potential of an anti-CD79b antibody-drug conjugate, anti-CD79b-vc-MMAE, for the treatment of non-Hodgkin lymphoma. Blood. 2009;114(13):2721-2729.

14. Antonow D, Thurston DE. Synthesis of DNA-interactive pyrrolo[2,1-c][1,4]benzodiazepines (PBDs). Chem Rev. 2011;111(4):2815-2864.

15. Hartley JA, Flynn MJ, Bingham JP, et al. Pre-clinical pharmacology and mechanism of action of SG3199, the pyrrolobenzodiazepine (PBD) dimer warhead component of antibody-drug conjugate (ADC) payload tesirine. Sci Rep. 2018;8(1):10479.

16. Caimi PF, Ai W, Alderuccio JP, et al. Loncastuximab tesirine in relapsed or refractory diffuse large B-cell lymphoma (LOTIS-2): a multicentre, open-label, single-arm, phase 2 trial. Lancet Oncol. 2021;22(6):790-800.

17. Hamadani M, Radford J, Carlo-Stella C, et al. Final results of a phase 1 study of loncastuximab tesirine in relapsed/refractory B-cell non-Hodgkin lymphoma. Blood. 2021;137(19):2634-2645.

18. Jain N, Stock W, Zeidan A, et al. Loncastuximab tesirine, an anti-CD19 antibody-drug conjugate, in relapsed/refractory B-cell acute lymphoblastic leukemia. Blood Adv. 2020;4(3):449-457.

19. Caimi PF, Ai WZ, Alderuccio JP, et al. Loncastuximab tesirine in relapsed/refractory diffuse large B-cell lymphoma: long-term efficacy and safety from the phase 2 LOTIS-2 study. Haematologica. 2024;109(4):1184-1193.

20. Calabretta E, Hamadani M, Zinzani PL, Caimi P, Carlo-Stella C. The antibody-drug conjugate loncastuximab tesirine for the treatment of diffuse large B-cell lymphoma. Blood. 2022;140(4):303-308.

21. Boi M, Gaudio E, Bonetti P, et al. The BET Bromodomain Inhibitor OTX015 Affects Pathogenetic Pathways in Preclinical B-cell Tumor Models and Synergizes with Targeted Drugs. Clin Cancer Res. 2015;21(7):1628-1638.

22. Golay J, Semenzato G, Rambaldi A, et al. Lessons for the clinic from rituximab pharmacokinetics and pharmacodynamics. MAbs. 2013;5(6):826-837.

23. Habermann TM, Weller EA, Morrison VA, et al. Rituximab-CHOP versus CHOP alone or with maintenance rituximab in older patients with diffuse large B-cell lymphoma. J Clin Oncol. 2006;24(19):3121-3127.

24. de Jong MRW, Langendonk M, Reitsma B, et al. Heterogeneous Pattern of Dependence on Anti-Apoptotic BCL-2 Family Proteins upon CHOP Treatment in Diffuse Large B-Cell Lymphoma. Int J Mol Sci. 2019;20(23):6036.

25. Spriano F, Tarantelli C, Cascione L, et al. Targeting CD25-positive lymphoma cells with the antibody-drug conjugate camidanlumab tesirine as single agent or in combination with targeted agents. bioRxiv. 2023:2023.07.02.547392. [preprint, not yet peer-reviewed]

26. Tarantelli C, Gaudio E, Arribas AJ, et al. PQR309 Is a Novel Dual PI3K/mTOR Inhibitor with Preclinical Antitumor Activity in Lymphomas as a Single Agent and in Combination Therapy. Clin Cancer Res. 2018;24(1):120-129.

27. Johnson Z, Tarantelli C, Civanelli E, et al. IOA-244 is a Non-ATP-competitive, Highly Selective, Tolerable PI3K Delta Inhibitor That Targets Solid Tumors and Breaks Immune Tolerance. Cancer Res Commun. 2023;3(4):576-591.

28. Hicks SW, Tarantelli C, Wilhem A, et al. The novel CD19-targeting antibody-drug conjugate huB4-DGN462 shows improved anti-tumor activity compared to SAR3419 in CD19-positive lymphoma and leukemia models. Haematologica. 2019;104(8):1633-1639.

29. Ran D, Moharil J, Lu J, et al. Platform comparison of HTG EdgeSeq and RNA-Seq for gene expression profiling of tumor tissue specimens. J Clin Oncol. 2020;38(15):3566.

30. Caimi PF, Hamadani M, Carlo-Stella C, et al. In relapsed or refractory diffuse large B-cell lymphoma, CD19 expression by immunohistochemistry alone is not a predictor of response to loncastuximab tesirine. EJHaem. 2024;5(1):76-83.

31. Arribas AJ, Napoli S, Cascione L, et al. Resistance to PI3κδ inhibitors in marginal zone lymphoma can be reverted by targeting the IL-6/PDGFRA axis. Haematologica. 2022;107(11):2685-2697.

32. Wang SS, Arribas AJ, Tarantelli C, et al. PI3K and BTK Inhibition Induces the Upregulation of CD19 and Increases Sensitivity to CAR T Cells in a Model of Marginal Zone Lymphoma (MZL). Blood. 2022;140(Supplement 1):4554-4555.

33. Curti L, Campaner S. MYC-Induced Replicative Stress: A Double-Edged Sword for Cancer Development and Treatment. Int J Mol Sci. 2021;22(12):6168.

34. Mantaj J, Jackson PJ, Rahman KM, Thurston DE. From Anthramycin to Pyrrolobenzodiazepine (PBD)-Containing Antibody-Drug Conjugates (ADCs). Angew Chem Int Ed Engl. 2017;56(2):462-488.

35. Mao S, Chaerkady R, Yu W, et al. Resistance to Pyrrolobenzodiazepine Dimers Is Associated with SLFN11 Downregulation and Can Be Reversed through Inhibition of ATR. Mol Cancer Ther. 2021;20(3):541-552.

36. Alderuccio JP, Ai WZ, Radford J, et al. Loncastuximab tesirine in relapsed/refractory high-grade B-cell lymphoma: a subgroup analysis from the LOTIS-2 study. Blood Adv. 2022;6(16):4736-4739.

37. Blanc V, Bousseau A, Caron A, Carrez C, Lutz RJ, Lambert JM. SAR3419: an anti-CD19-Maytansinoid Immunoconjugate for the treatment of B-cell malignancies. Clin Cancer Res. 2011;17(20):6448-6458.

38. Amin DN, Bannerji R, Mali RS, et al. Abstract CT133: Targeting BCL-2 and MCL-1 overcomes treatment resistance in relapsed and refractory non-Hodgkin lymphoma: Pre-clinical rationale and results from an open-label phase 1b study. Cancer Res. 2020;80(16_Supplement):CT133.

39. Gaudio E, Tarantelli C, Spriano F, et al. Targeting CD205 with the antibody drug conjugate MEN1309/OBT076 is an active new therapeutic strategy in lymphoma models. Haematologica. 2020;105(11):2584-2591.

40. Chiou JT, Huang NC, Huang CH, et al. NOXA-mediated degradation of MCL1 and BCL2L1 causes apoptosis of daunorubicin-treated human acute myeloid leukemia cells. J Cell Physiol. 2021;236(11):7356-7375.

41. Zelenetz AD, Jurczak W, Ribrag V, et al. Efficacy and Safety of Single-Agent Zandelisib Administered By Intermittent Dosing in Patients with Relapsed or Refractory (R/R) Follicular Lymphoma (FL): Final Results of the Tidal Phase 2 Study. Blood. 2022;140(Supplement 1):3595-3597.

42. Carlo-Stella C, Tarantelli C, Civanelli E, et al. Highly Selective Allosteric Modulator of the Phosphoinositide 3-Kinase Delta (PI3Kδ) Roginolisib In Patients With Refractory/Relapsed Follicular Lymphoma. Hematol Oncol. 2023;41(S2):574-574.

43. Brown JR, Danilov AV, LaCasce AS, Davids MS. PI3K inhibitors in haematological malignancies. Lancet Oncol. 2022 Aug;23(8):e364.

44. Cucchi D, Sachini N, van Berkel PH, Zammarchi F. Abstract 1050: Mechanistic studies investigating the synergistic combination of Loncastuximab Tesirine and Ibrutinib in pre-clinical models of B-cell non-Hodgkin lymphoma. Cancer Res. 2022;82(12_Supplement):1050.

45. Depaus J, Wagner-Johnston N, Zinzani PL, et al. Clinical Activity of Loncastuximab Tesirine Plus Ibrutinib in Non-Hodgkin Lymphoma: Updated Lotis 3 Phase 1 Results. Hematol Oncol. 2021;39(S2):325.

46. Zhong H, Chen C, Tammali R, et al. Improved Therapeutic Window in BRCA-mutant Tumors with Antibody-linked Pyrrolobenzodiazepine Dimers with and without PARP Inhibition. Mol Cancer Ther. 2019;18(1):89-99.

47. Zammarchi F, Havenith KE, Chivers S, et al. Preclinical Development of ADCT-601, a Novel Pyrrolobenzodiazepine Dimer-based Antibody-drug Conjugate Targeting AXL-expressing Cancers. Mol Cancer Ther. 2022;21(4):582-593.

48. Fusani S, Rossi A, Mazzara S, et al. CD19-Mediated DNA Damage Boost in Lymphoma Cells Treated with Loncastuximab Tesirine in Combination with PARP Inhibitors. Blood. 2021;138(Supplement 1):1342.

49. Parvin S, Ramirez-Labrada A, Aumann S, et al. LMO2 Confers Synthetic Lethality to PARP Inhibition in DLBCL. Cancer Cell. 2019;36(3):237-249.

50. Carrassa L, Colombo I, Damia G, Bertoni F. Targeting the DNA damage response for patients with lymphoma: Preclinical and clinical evidences. Cancer Treat Rev. 2020;90:102090.

51. Soumerai JD, Zelenetz AD, Moskowitz CH, et al. The PARP Inhibitor Veliparib Can Be Safely Added to Bendamustine and Rituximab and Has Preliminary Evidence of Activity in B-Cell Lymphoma. Clin Cancer Res. 2017;23(15):4119-4126.

52. Strati P, Neelapu SS. CAR-T failure: beyond antigen loss and T cells. Blood. 2021;137(19):2567-2568.

53. Caimi PF, Ardeshna KM, Reid E, et al. The AntiCD19 Antibody Drug Immunoconjugate Loncastuximab Achieves Responses in DLBCL Relapsing After AntiCD19 CAR-T Cell Therapy. Clin Lymphoma Myeloma Leuk. 2022;22(5):e335-e339.

54. Horvei P, Sakemura R, Cox MJ, et al. Targeting of CD19 By Tafasitamab Does Not Impair CD19 Directed Chimeric Antigen Receptor T Cell Activity in Vitro. Biol Blood Marrow Transplant. 2020;26(3):S223-S224.

55. Tabbara N, Gaut D, Oliai C, Lewis T, de Vos S. Anti-CD19 CAR T-cell therapy remission despite prior anti-CD19 antibody Tafasitamab in relapsed/refractory DLBCL. Leuk Res Rep. 2021;16:100260.

56. Thapa B, Caimi PF, Ardeshna KM, et al. CD19 antibody-drug conjugate therapy in DLBCL does not preclude subsequent responses to CD19-directed CAR T-cell therapy. Blood Adv. 2020;4(16):3850-3852.

57. Dodero A, Bramanti S, Di Trani M, et al. Outcome after chimeric antigen receptor (CAR) T-cell therapy failure in large B-cell lymphomas. Br J Haematol. 2024;204(1):151-159.

## Tables

**Table 1. Anti-tumor activity of loncastuximab tesirine in lymphoma cell lines.** $IC_{50}$ values were obtained after 96 hours of treatment. DLBCL, diffuse large B-cell lymphoma; ABC, activated B cell; GCB, germinal center B cell; MCL, mantle cell lymphoma; MZL, marginal zone lymphoma; CLL, chronic lymphocytic leukemia; HL, Hodgkin lymphoma; PMBCL, primary mediastinal large B cell lymphoma; CTCL, cutaneous T cell lymphoma; ALCL, anaplastic large cell lymphoma; PTCL-NOS, peripheral T cell lymphoma-not otherwise specified. n.d., not determined. * The upper confidence limit was held at a maximum for the sample.

| | No. | Median $IC_{50}$ (pM) | 95% confidence interval (pM) |
|---|---|---|---|
| ABC DLBCL | 7 | 35 | 7.3-880 |
| GCB DLBCL | 19 | 2 | 1.17-10.6 |
| MCL | 10 | 1.75 | 1.1-5.4 |
| MZL | 6 | 2.5 | 0.47-496 |
| CLL | 2 | 15.75 | 5.5-26 * |
| HL | 3 | 2750 | 600-14000 * |
| PMBCL | 1 | 1.5 | n.d. |
| ALCL | 4 | 4875 | 700-11500 * |
| CTCL | 4 | 2500 | 900-35000 * |
| PTCL-NOS | 1 | 850 | n.d. |

**Table 2. Anti-tumor activity of the SG3199 warhead in lymphoma cell lines.** $IC_{50}$ values were obtained after 96 hours of treatment. DLBCL, diffuse large B-cell lymphoma; ABC, activated B cell; GCB, germinal center B cell; MCL, mantle cell lymphoma; MZL, marginal zone lymphoma; CLL, chronic lymphocytic leukemia; HL, Hodgkin lymphoma; PMBCL, primary mediastinal large B-cell lymphoma; CTCL, cutaneous T cell lymphoma; ALCL, anaplastic large cell lymphoma; PTCL-NOS, peripheral T cell lymphoma-not otherwise specified. n.d., not determined. * Upper confidence limit held at a maximum of the sample.

| | No. | Median $IC_{50}$ (pM) | 95% confidence interval (pM) |
|---|---|---|---|
| ABC DLBCL | 7 | 1.17 | 0.63-7.85 |
| GCB DLBCL | 19 | 1.14 | 0.75-1.53 |
| MCL | 10 | 0.53 | 0.53-1.66 |
| MZL | 6 | 0.53 | 0.53-0.85 |
| CLL | 2 | 0.83 | 0.53-1.14* |
| HL | 3 | 4.97 | 0.85-29.24* |
| PMBCL | 1 | 0.56 | n.d. |
| ALCL | 4 | 2.34 | 0.85-17.54* |
| CTCL | 4 | 1.59 | 0.53-23.39* |
| PTCL-NOS | 1 | 0.53 | n.d. |

**Table 3. Loncastuximab tesirine containing combinations in DLBCL and MCL cell lines**; ABC DLBCL, activated B cell like diffuse large B cell lymphoma; GCB DLBCL, germinal center B cell like diffuse large B cell lymphoma; MCL, mantle cell lymphoma.

| Combination Partner | Histology | Cell line | Median Chou-Talalay combination index | 95% confidence interval |
|---|---|---|---|---|
| Venetoclax | ABC DLBCL | OCI-Ly-3 | 0.48 | 0.3-0.6 |
| | ABC DLBCL | TMD8 | 0.63 | 0.48-1.17 |
| | GCB DLBCL | VAL | 0.75 | 0.66-0.91 |
| | GCB DLBCL | WSU-DLCL2 | 0.4 | 0.19-1.86 |
| | MCL | JVM2 | 0.37 | 0.25-0.69 |
| | MCL | JEKO-1 | 0.88 | 0.37-1.01 |
| Copanlisib | ABC DLBCL | OCI-Ly-3 | 0.53 | 0.41-0.68 |
| | ABC DLBCL | TMD8 | 1.07 | 0.52-1.22 |
| | GCB DLBCL | VAL | 0.84 | 0.63-0.93 |
| | GCB DLBCL | WSU-DLCL2 | 1.56 | 0.87-1.80 |
| | MCL | JVM2 | 0.19 | 0.09-0.47 |
| | MCL | JEKO-1 | 0.75 | 0.41-1.05 |
| Idelalisib | ABC DLBCL | OCI-Ly-3 | 0.1 | 0.07-0.22 |
| | ABC DLBCL | TMD8 | 0.9 | 0.41-1.24 |
| | GCB DLBCL | VAL | 0.86 | 0.67-1.22 |
| | GCB DLBCL | WSU-DLCL2 | 0.5 | 0.30-0.75 |
| | MCL | JVM2 | 0.42 | 0.36-0.79 |
| | MCL | JEKO-1 | 1.32 | 0.68-1.65 |
| Bendamustine | ABC DLBCL | OCI-Ly-3 | 1 | 0.7-1.75 |
| | ABC DLBCL | TMD8 | 0.6 | 0.35-1.92 |
| | GCB DLBCL | VAL | 0.89 | 0.59-1.14 |
| | GCB DLBCL | WSU-DLCL2 | 0.62 | 0.51-0.83 |
| Bortezomib | ABC DLBCL | OCI-Ly-3 | >3 | >3 |
| | ABC DLBCL | TMD8 | 1.13 | 0.86-1.57 |
| Ibrutinib | ABC DLBCL | OCI-Ly-3 | 0.76 | 0.39-0.9 |
| | ABC DLBCL | TMD8 | 1.07 | 0.96-1.25 |
| Lenalidomide | ABC DLBCL | OCI-Ly-3 | 1.58 | 0.82-4.08 |
| | ABC DLBCL | TMD8 | 1.88 | 0.93-2.36 |
| Olaparib | ABC DLBCL | OCI-Ly-3 | 1.41 | 0.99-2.06 |
| | ABC DLBCL | TMD8 | 0.95 | 0.41-1.29 |
| | GCB DLBCL | VAL | 0.86 | 0.67-1.22 |
| | GCB DLBCL | WSU-DLCL2 | 0.5 | 0.30-0.75 |
| Rituximab | ABC DLBCL | OCI-Ly-3 | >3 | >3 |
| | ABC DLBCL | TMD8 | >3 | >3 |
| | GCB DLBCL | VAL | 0.09 | 0.06-0.14 |
| | GCB DLBCL | WSU-DLCL2 | >3 | >3 |

**Legend to Figures**

**Figure 1. The *in vitro* anti-proliferative activities of loncastuximab tesirine correlated with CD19 expression.** Pearson correlations between loncastuximab tesirine activity with CD19 protein absolute (A) and relative (B) expression, CD19 transcript measured with the Illumina HT-12 arrays (C), HTG biomarker panel (D) and total RNASeq data (E).

**Figure 2. Correlation between the activity of loncastuximab tesirine and its warhead SG3199.** Pearson correlations between loncastuximab tesirine and SG3199 $IC_{50}$ values across all cell lines (A) and in cell lines derived from B cell lymphomas and Hodgkin lymphoma (HL) (B).

**Figure 3. Correlation between the activity of loncastuximab tesirine or its warhead SG3199 and R-CHOP in diffuse large B-cell lymphoma (DLBCL) cell lines.** Pearson correlations between R-CHOP and loncastuximab tesirine (A) or SG3199 (B).

**Figure 4. Proteins modulated after exposure to loncastuximab tesirine.** Representative immunoblots from one ABC DLBCL (TMD8) and one GCB DLBCL (WSU-DLCL2) cell lines treated for 24 hours with drugs as single or the combination of loncastuximab tesirine with venetoclax, idelalisib and copanlisib at concentrations corresponding to two times the $IC_{50}$ values.

**Figure 5. The combination of loncastuximab tesirine plus copanlisib and venetoclax is *in vivo* superior to single agents in ABC DLBCL and mantle cell lymphoma (MCL) xenograft model.** (A) NOD-SCID Mice were subcutaneously (sc) injected with TMD8 and treated (n.=9 per group) with loncastuximab tesirine and copanlisib as single agents and in combination, and, as control with vehicle (PBS) or the non-binding control ADC B12-SG3249 (n.=4 per group). * q values < 0.01 of combo vs all other groups (vehicle, B12-SG3249, loncastuximab tesirine, copanlisib) was determined by Mann-Whitney test followed by two-stage step-up (Benjamini, Krieger, and Yekutieli) multiple comparisons, FDR(q)=0.01.
(B) NSG mice were sc injected with JEKO1 and treated (n.=8 per group) with loncastuximab tesirine and venetoclax as single agents and in combination, and PBS as control. Y-axis average tumor volume expressed in $mm^3$ ± SEM. * q values < 0.01 of combo vs vehicle and loncastuximab tesirine group, as determined by Mann-Whitney test followed by two-stage step-up (Benjamini, Krieger, and Yekutieli) multiple comparisons, FDR(q)=0.01. False discovery rate, FDR.

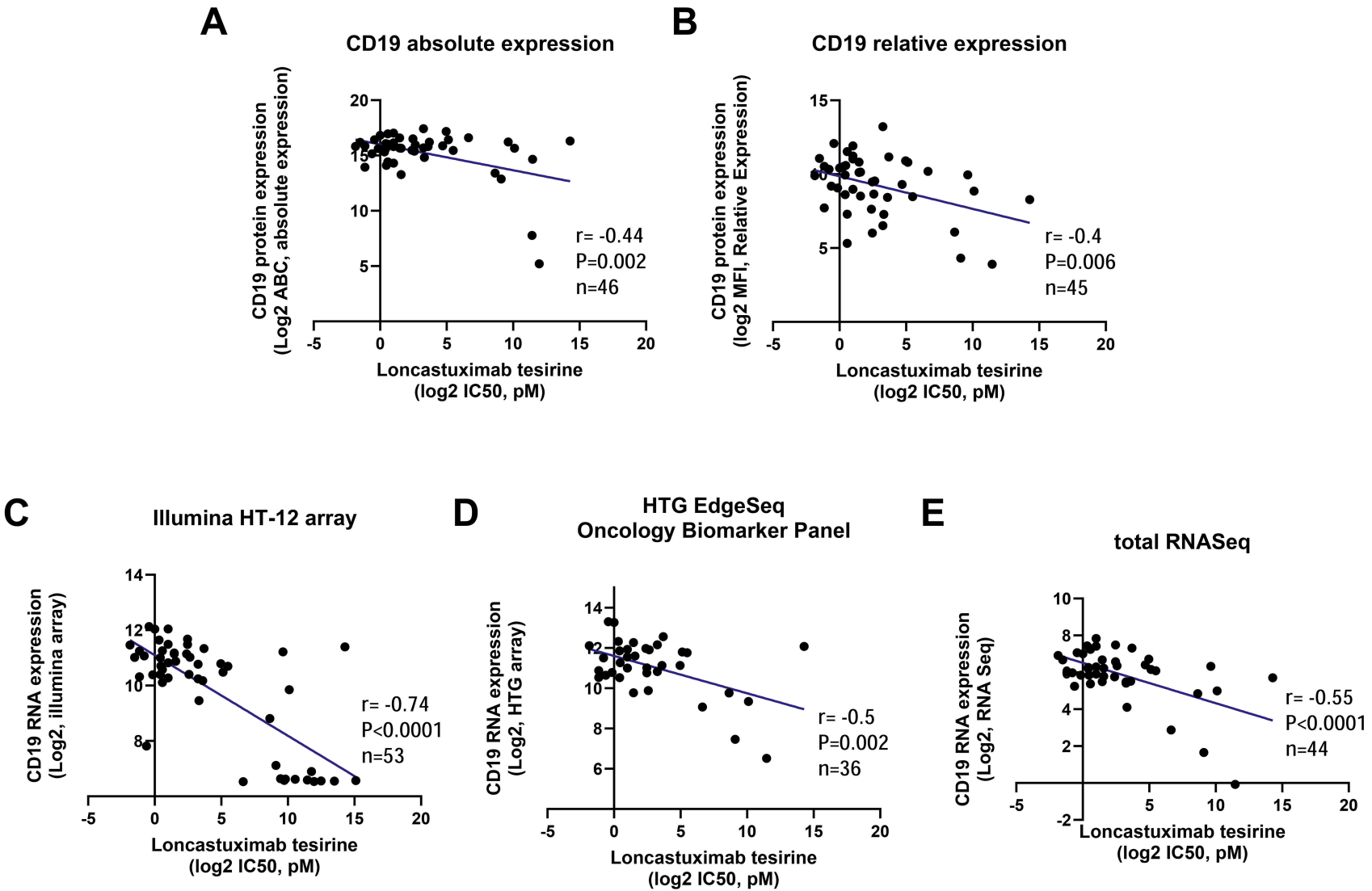
A
CD19 absolute expression
CD19 protein expression
(Log2 ABC, absolute expression)
r= -0.44
P=0.002
n=46
Loncastuximab tesirine
(log2 IC50, pM)
B
CD19 relative expression
CD19 protein expression
(log2 MFI, Relative Expression)
r= -0.4
P=0.006
n=45
Loncastuximab tesirine
(log2 IC50, pM)
C
Illumina HT-12 array
CD19 RNA expression
(Log2, illumina array)
r= -0.74
P<0.0001
n=53
Loncastuximab tesirine
(log2 IC50, pM)
D
HTG EdgeSeq
Oncology Biomarker Panel
CD19 RNA expression
(Log2, HTG array)
r= -0.5
P=0.002
n=36
Loncastuximab tesirine
(log2 IC50, pM)
E
total RNASeq
CD19 RNA expression
(Log2, RNA Seq)
r= -0.55
P<0.0001
n=44
Loncastuximab tesirine
(log2 IC50, pM)

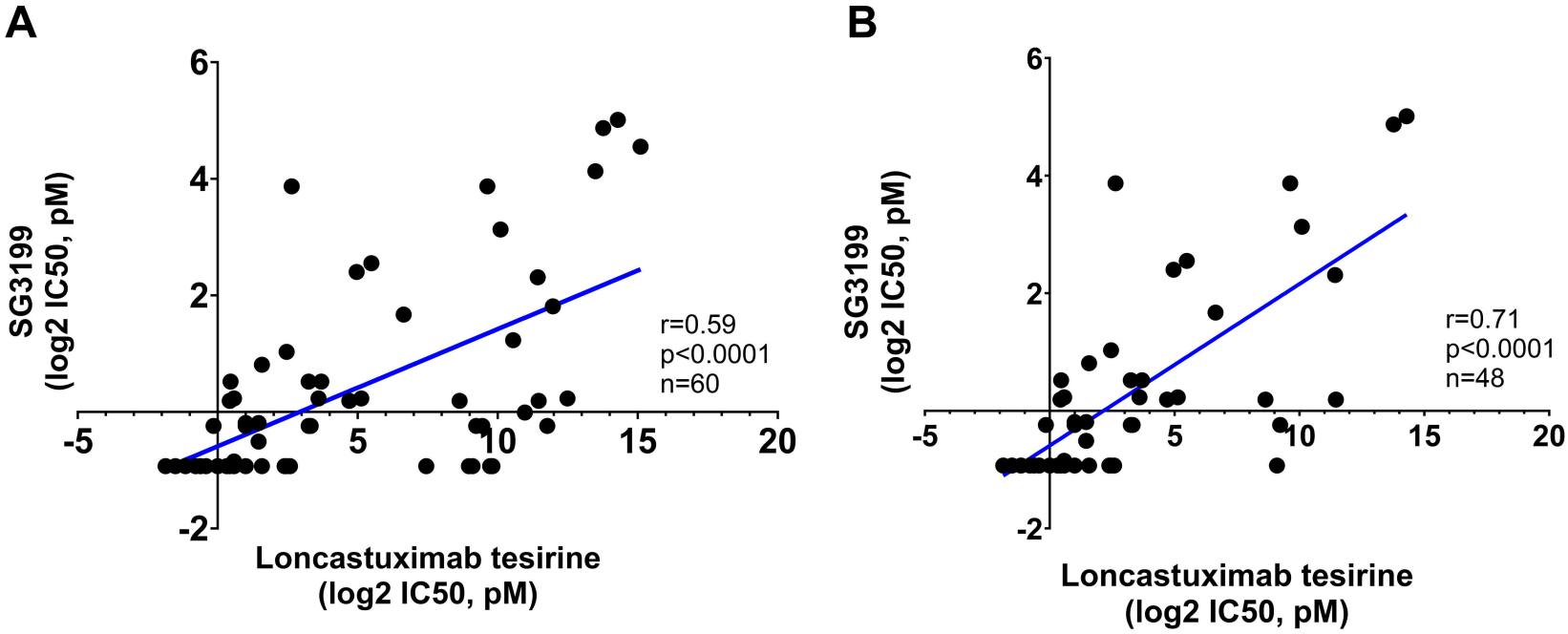
A
SG3199
(log2 IC50, pM)
6
4
2
-2
-5
5
10
15
20
r=0.59
p<0.0001
n=60
Loncastuximab tesirine
(log2 IC50, pM)
B
SG3199
(log2 IC50, pM)
6
4
2
-2
-5
5
10
15
20
r=0.71
p<0.0001
n=48
Loncastuximab tesirine
(log2 IC50, pM)

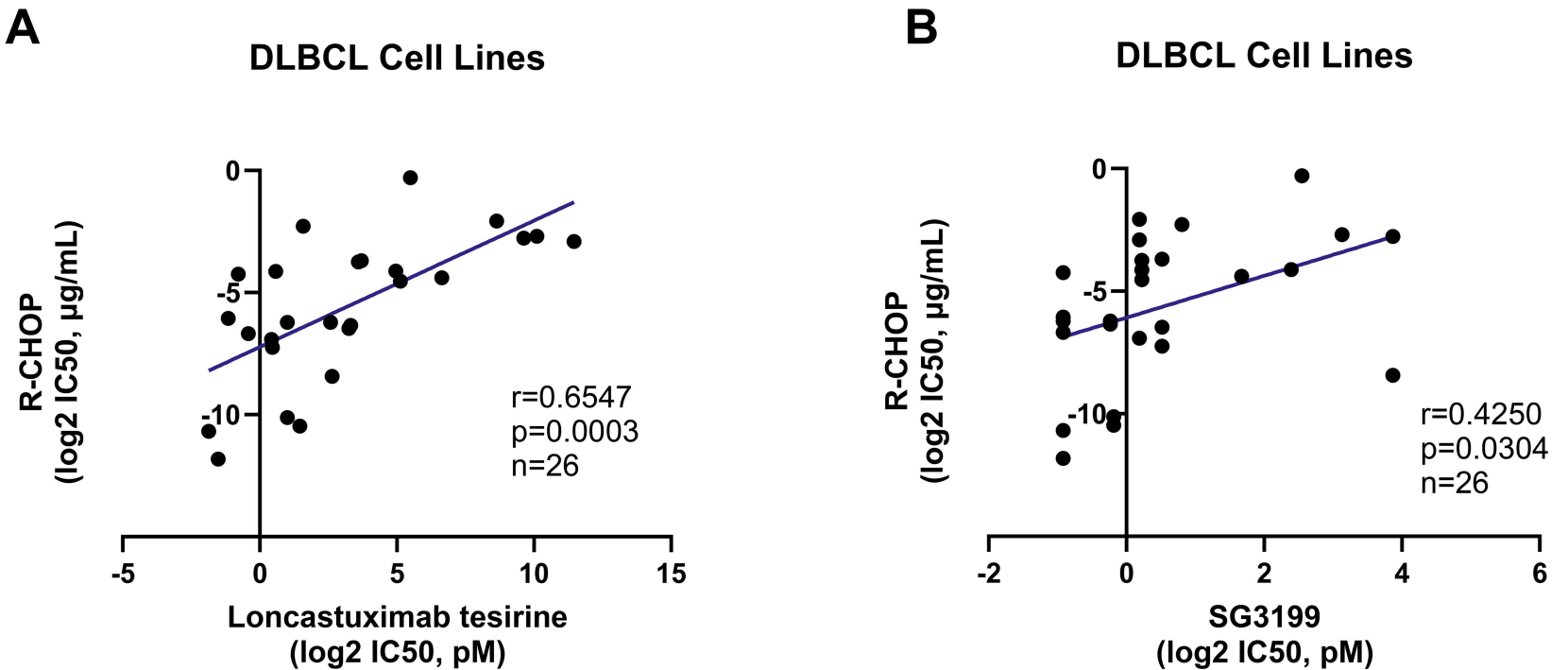
A
DLBCL Cell Lines
R-CHOP
(log2 IC50, µg/mL)
0
-5
-10
-5
0
5
10
15
r=0.6547
p=0.0003
n=26
Loncastuximab tesirine
(log2 IC50, pM)
B
DLBCL Cell Lines
R-CHOP
(log2 IC50, µg/mL)
0
-5
-10
-2
0
2
4
6
r=0.4250
p=0.0304
n=26
SG3199
(log2 IC50, pM)

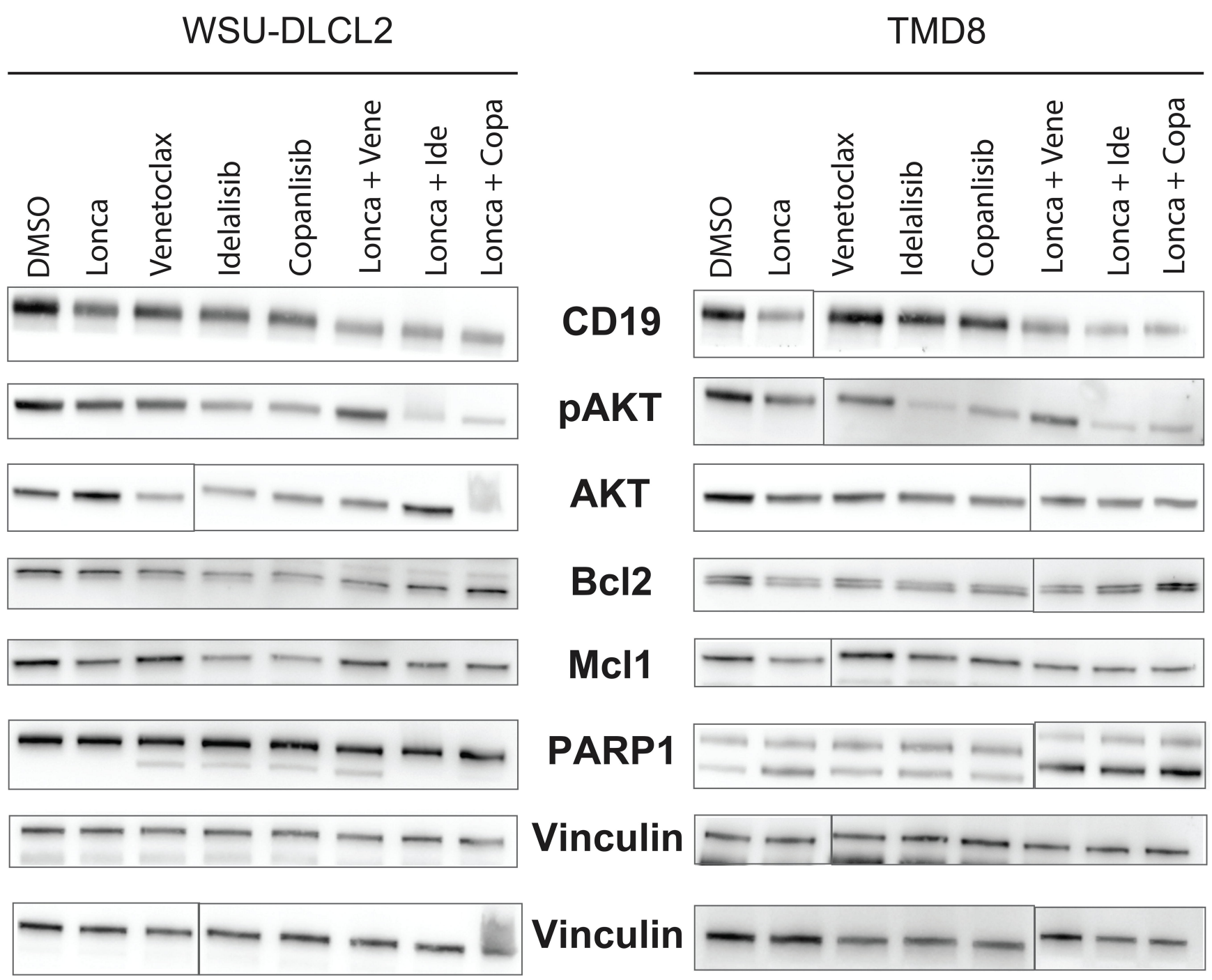
WSU-DLCL2
TMD8
DMSO
Lonca
Venetoclax
Idelalisib
Copanlisib
Lonca + Vene
Lonca + Ide
Lonca + Copa
CD19
pAKT
AKT
Bcl2
Mcl1
PARP1
Vinculin
Vinculin

A

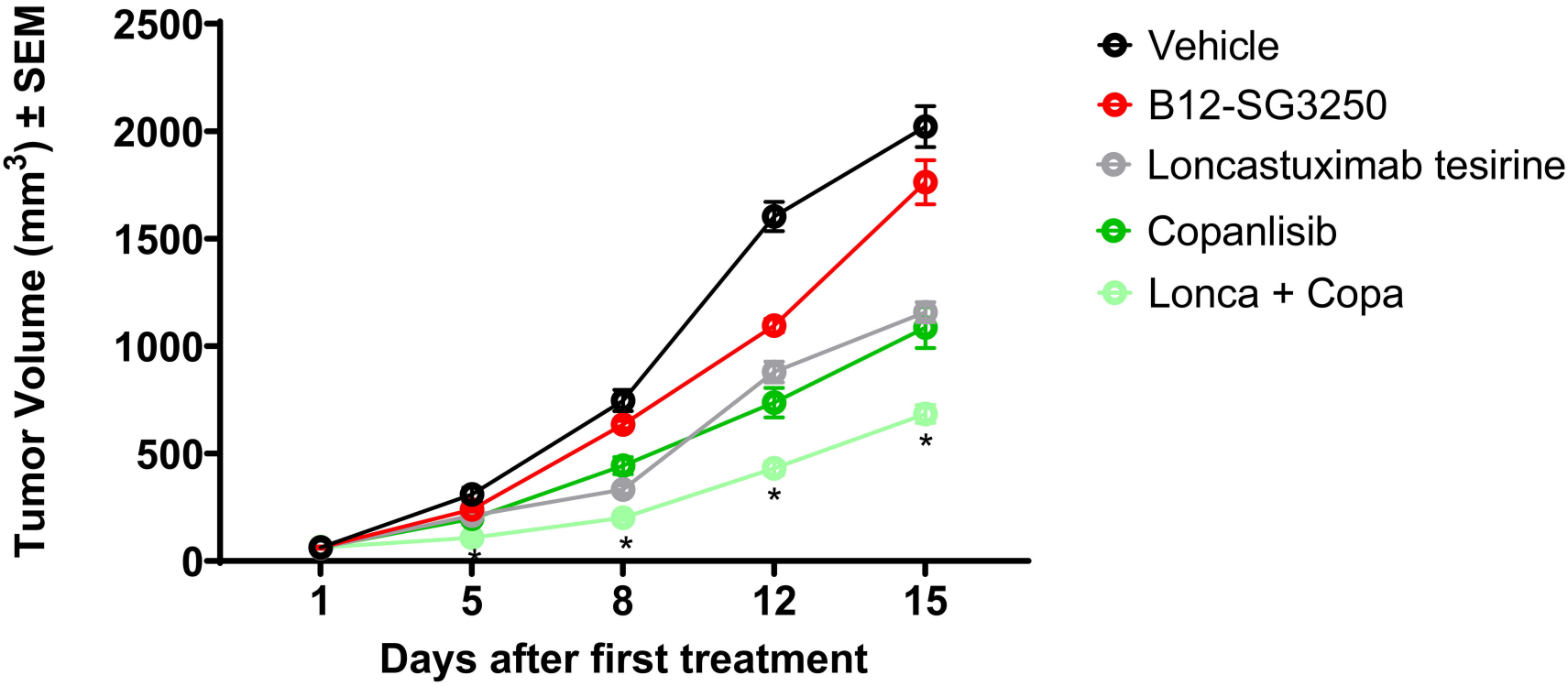
TMD8 xenograft
Tumor Volume (mm3) ± SEM
2500
2000
1500
1000
500
0
1
5
8
12
15
Days after first treatment
*
*
*
*
Vehicle
B12-SG3250
Loncastuximab tesirine
Copanlisib
Lonca + Copa

B

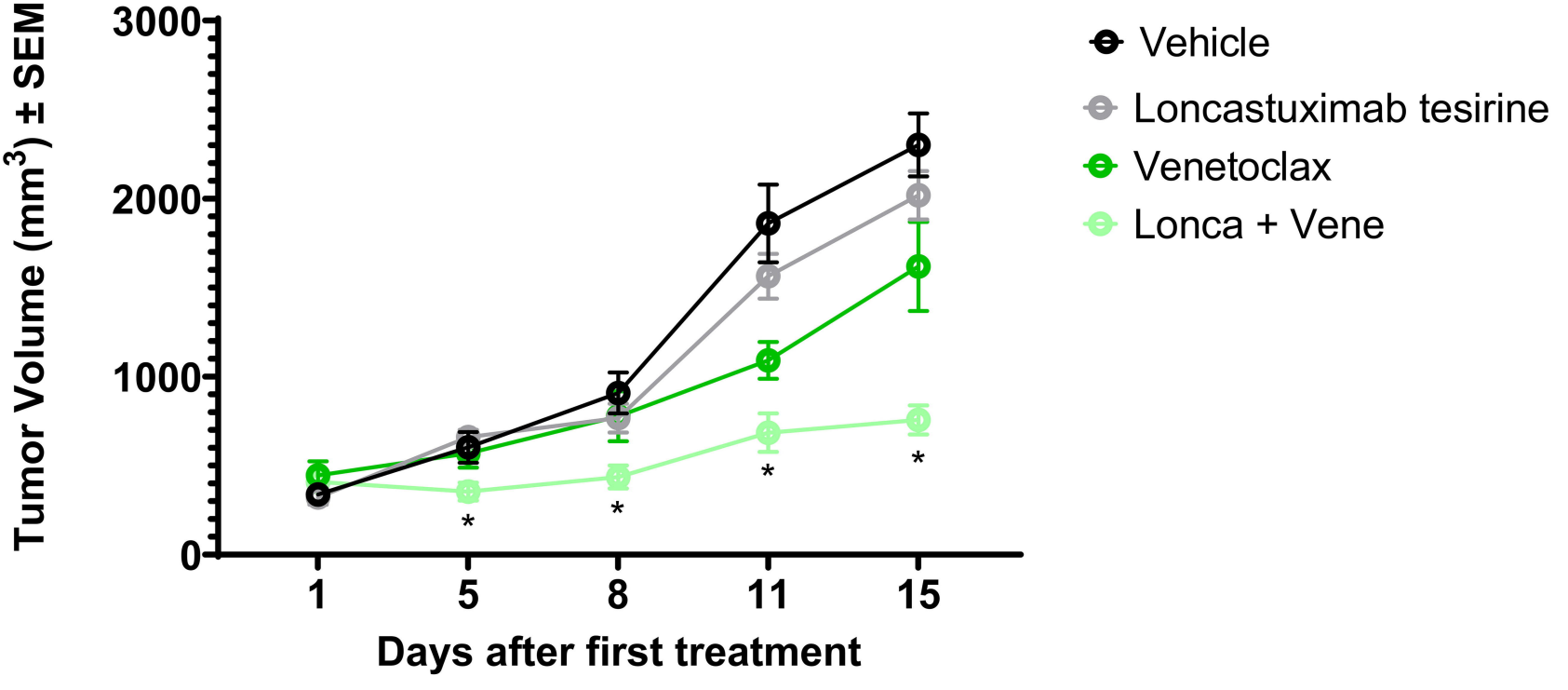
JEKO1 xenograft
Tumor Volume (mm3) ± SEM
3000
2000
1000
0
1
5
8
11
15
Days after first treatment
*
*
*
*
Vehicle
Loncastuximab tesirine
Venetoclax
Lonca + Vene

**Targeting CD19-positive lymphomas with the antibody-drug conjugate loncastuximab tesirine: preclinical evidence as single agent and in combination therapy**

Chiara Tarantelli* [1^], David Wald [2^], Nicolas Munz [1], Filippo Spriano [1], Alessio Bruscaggin [1], Eleonora Cannas [1], Luciano Cascione [1,3], Eugenio Gaudio [1], Alberto J. Arribas [1,3], Shivaprasad Manjappa [4], Gaetanina Golino [1], Lorenzo Scalise [1], Maria Teresa Cacciapuoti [5], Emanuele Zucca [1,6], Anastasios Stathis [6,7], Giorgio Inghirami [5], Patrick H. van Berkel [8], Davide Rossi [1,6], Paolo F. Caimi [9], Francesca Zammarchi [8], Francesco Bertoni* [1,6]

[1] *Institute of Oncology Research, Faculty of Biomedical Sciences, USI, Bellinzona, Switzerland;*
[2] *Case Western Reserve University, Cleveland, OH, USA;*
[3] *SIB Swiss Institute of Bioinformatics, Lausanne, Switzerland;*
[4] *Fred Hutchinson Cancer Center, Seattle, Washington, USA;*
[5] *Department of Pathology and Laboratory Medicine, Weill Cornell Medicine, New York, NY;*
[6] *Oncology Institute of Southern Switzerland, Ente Ospedaliero Cantonale, Bellinzona, Switzerland;*
[7] *Faculty of Biomedical Sciences, USI, Lugano, Switzerland;*
[8] *ADC Therapeutics (UK) Ltd., London, UK;*
[9] *Cleveland Clinic/Case Comprehensive Cancer Center, Cleveland, OH, USA.*

## Supplementary materials and methods

Cell lines

Lymphoma cell lines were cultured according to the recommended conditions, as previously described [1]. All media were supplemented with fetal bovine serum (10% or 20%) and penicillin-streptomycin-neomycin (≈5,000 units penicillin, 5 mg streptomycin, and 10 mg neomycin/mL; Sigma). Human cell line identities were confirmed by short tandem repeat DNA fingerprinting using the Promega GenePrint 10 System kit (B9510). Cells were periodically tested for mycoplasma negativity using the MycoAlert Mycoplasma Detection Kit (Lonza).

Compounds

Loncastuximab tesirine, SG3199 and B12-SG3249 were provided by ADC Therapeutics. Copanlisib was purchased from MedKoo Biosciences Inc. (Morrisville, NC, USA). Idelalisib, venetoclax, bendamustine, olaparib, ibrutinib, doxorubicin, vincristine, prednisolone, bortezomib, and lenalidomide were purchased from Selleckchem (Houston, TX, USA). Rituximab was purchased from Roche (Basel, Switzerland), and 4-hydroperoxy-cyclophosphamide from Santa Cruz Biotechnology (Heidelberg, Germany).

Patient-derived xenograft (PDX) cell line

PDX was first digested and then passed through 70µm nylon filters. Cell suspension was washed twice with PBS, and dead cells were removed using the Ficoll gradient. Viable cells were then cultured in RPMI (Sigma) supplemented with 20% FBS (Corning), 100 U/ml glutamine (Sigma), Normocin 1:500 (InvivoGen), and 100µg/ml streptomycin (Sigma) and maintained at 37°C in a humidified 5% CO2 atmosphere [2]. PDX-Dlines media was initially supplemented with exogenous IL-2 (50U/ml), IL6 (10µg/ml), and IL10 (20µg/ml). Exogenous lymphokines were ultimately excluded when possible. PDX-Dline was analyzed by flow cytometry using a panel of monoclonal antibodies against human pan B- or T-cell surface markers twice per year. Genotyping was performed once a year (biosynthesis, Tx). PDX was produced in the context of protocols approved by the Cornell University (IRB: 107004999, 0201005295 and 1410015560; Universal consent: 1302013582; *in vivo* protocol 2014-0024).
To determine the expression of CD19, 1x106 cells were pre-incubated with FcR blocking reagent (catalog no. 130-059-901; Miltenyi Biotec, Bisley, UK) to prevent unspecific binding of staining antibodies, following manufacturer's instructions, and then stained with anti-Hu-CD19 antibody (BD Biosciences, BD Pharmingen PE Mouse Anti-human CD19-555413) or with the isotype (BD Pharminge PE Mouse IgG1, κ Isotype Control-555749). Median Fluorescence Intensities were acquired in a BD

LSRFortessa instrument (BD Biosciences, Allschwil, Switzerland), and data were analyzed using FlowJo software (TreeStar Inc., Ashland, OR USA).

LyV4.0 CAPP-seq gDNA Assay and variant calling

Genomic DNA was extracted from cell lines using the DNeasy Blood & Tissue Kits (Qiagen, Hilden, Germany). Library preparation started with shearing at least 500 ng of DNA through sonication (Covaris, Woburn, MA) to obtain 100 to 200 bp fragments. The gDNA libraries were then generated with the KAPA Hyper Prep Kit (KAPA Biosystems). The regions of interest (Table S1) were enriched using SeqCap HyperChoice Library probes (NimbleGen; Roche Diagnostics, Jakarta, Indonesia). Libraries were sequenced on the NextSeq500 (Illumina, San Diego, CA) instrument by paired-end sequencing (2 × 150-cycle protocol). A total of 52 multiplexed libraries were simultaneously sequenced in each deep experiment. Sequencing reads in FASTQ format were deduplicated utilizing FastUniq v1.1. The resulting reads were locally aligned to the hg19 human genome assembly using the BWA-MEM v.0.7.17 software with the default settings and then sorted, indexed, and assembled into a mpileup file using SAMtools v.1.7. The aligned reads were processed with mpileup using the parameters -A -d 10 000 000. Single nucleotide variations and indels were called in gDNA with the mpileupCNS function of VarScan2 (v.2.2.4) using the parameters min-coverage 1 --min-coverage-normal 1 --min-coverage-tumor 1 --min-var-freq 0 --min-freq-for-hom 0.75 --somatic-p-value 0.05 --min-avg-qual 30 --strand-filter 1 --validation 1 --output VCF. The variant called by VarScan2 was annotated using the Annovar software (wAannovar https://wannovar.wglab.org/). The analysis retained all the variants affecting coding regions or splice sites. All variants were systematically compared to online databases to confer the origin of somatic status. Somatic origin of non-synonymous single nucleotide variants (SNV) and/or inframe In/del was confirmed only if was detected as “somatic confirmed” in COSMIC database (https://cancer.sanger.ac.uk/cosmic), without a presence in polymorphisms database (https://www.ncbi.nlm.nih.gov/variation/view/ ; https://www.ncbi.nlm.nih.gov/variation/tools/1000genomes/); somatic status was also confirmed by the high damaging prediction score provided by poliphen2 and SIFT online software (http://genetics.bwh.harvard.edu/pph2/ ; https://sift.bii.a-star.edu.sg/www/SIFT4G_vcf_submit.html). Their non-presence in the polymorphisms' database was enough to call variants somatic for truncating variants, frameshift, splicing variants, and/or stop codons. An in-house database containing all gDNA background allele frequencies across gDNA samples from healthy subjects was used to filter out systematic sequencing errors in gDNA. Based on the assumption that all background allele fractions follow a normal distribution, a Z-test was employed to test whether a given variant in the gDNA differed significantly in its frequency from typical gDNA background at the same position in all gDNA samples after adjusting for multiple comparisons by Bonferroni test (multiple comparisons corrected p threshold corresponding to alpha of 0.05/[size of the target region in bp × 4 alleles per position]). Variants that did not pass these filters were not further considered. Variants for the resulting candidate mutations were visualized using Integrative Genomics Viewer. Genes mutational levels were correlated with loncastuximab tesirine drug activity quantified as $IC_{50}$ values by Mann Whitney test with STATA Stata/BE 17.0 (Stata Corporation, College Station, TX). P-value for significance was <0.05. For multiple correction analysis, a two-stage linear step-up procedure of Benjamini, Krieger, and Yekutieli was adopted with significance at a threshold of <0.05, using Prism software v8.0 (GraphPad Software La Jolla, CA, USA).

Immunoblotting

Cells were seeded in T25 flasks at a density of $5x10^5$ per mL and treated for 24 hours with DMSO or single drugs at their 2 times $IC_{50}$ concentrations or with loncastuximab tesirine plus venetoclax, idelalisib, or copanlisib. Protein extraction was performed by lysing the cells with M-PER (Mammalian Protein Extraction Reagent, ThermoFisher Scientific, Waltham, MA, USA) lysis buffer plus Halt Protease and Phosphatase Inhibitor Cocktail, EDTA-Free (100X) for 30 minutes on ice and then centrifuged at high speed and 4°C for 30 minutes. Protein concentration was determined using the BCA protein assay (Pierce Chemical Co, Dallas, TX, USA), and 30 μg of total proteins were loaded and

separated on a 4-20% gradient SDS-polyacrylamide gel by electrophoresis (SDS-PAGE). Proteins were transferred on nitrocellulose membranes and incubated with primary antibodies overnight, followed by the appropriate horseradish peroxidase–conjugated anti-mouse (NA931V) or anti-rabbit (NA934V) secondary antibodies (GE Healthcare, Chicago, IL, USA) for 1 hour at room temperature. Enhanced chemiluminescence detection was done following the manufacturer's instructions (Amersham Life Science). Luminescence is measured by the Fusion Solo S instrument (Witec AG, Sursee, Switzerland). Finally, protein quantification was performed using the Fusion Solo S instrument (Witec AG). Equal loading of samples was confirmed by probing for vinculin. The antibodies used for the experiment were: anti-Vinculin (Sigma Aldrich cat. n.V9131), anti-AKT (CST-9272), anti-p-AKT (Ser 473) (CST-4060), anti-CD19 (abcam-AB134114), anti-PARP1 (SC-8007), anti-Mcl1 (D35A5) (CST-5453) and anti-Bcl2 (SC-492) as primary antibodies.

Cell cycle

Cells were seeded in 96 wells-plates at a density of $10^4$ (OCI-LY-3) or $2x10^4$ (TMD8, VAL, WSU-DLCL2) per well and subsequently treated with single drugs or with the combination of loncastuximab tesirine plus venetoclax, idelalisib or copanlisib at 2 times $IC_{50}$ concentrations for 96 hours. Cells were fixed with 70% cold ethanol before staining with propidium Iodide (PI) and RNAse treatment. Acquisitions were carried out with a FACSCanto II instrument (BD Biosciences, Allschwil, Switzerland), and data were analyzed using FlowJo software (TreeStar Inc., Ashland, OR, USA).

Data mining

Statistical analyses were conducted using Prism software v8.0 (GraphPad Software La Jolla, CA, USA). For immunoblotting, cell proliferation, cell death, cell cycle, and apoptotic assay, statistical significance was determined by a two-tailed unpaired Student's t-test. A P value < 0.05 was considered statistically significant. *BCL2* and/or *MYC* translocations and *TP53* inactivation were retrieved from our previous publication [3]. Differences in $IC_{50}$ values among lymphoma subtypes were calculated using the Mann-Whitney test. P values of 0.05 or less defined statistical significance.

*In vivo* experiments

*TMD8 xenograft*: Mice maintenance and animal experiments were performed under the institutional guidelines established for the Animal Facility at The Institute of Research in Biomedicine (IRB) (license n. TI 49-2018). NOD-SCID mice were obtained from Charles River (Wilmington, MA, USA). Xenografts were established by injecting TMD8 lymphoma cells ($15 \times 10^6$ cells/mouse, 200 µL of PBS) into the left flanks of female NOD-SCID mice (6 weeks of age, approximately 20 grams of body weight). Treatments started with measurable tumors. Tumor volume (TV) was calculated using the equation V = [length x width x height]/2. The animal status was evaluated during housing and treatments by measuring the Body Condition Score (BSC) [4].

*JEKO1 xenograft:* Eight-week-old female Nod/SCID/IL2-Rg-/- (NSG) mice (Jackson Lab, Bar Harbor, Maine) were injected subcutaneously into both flanks with $10 \times 10^6$ Jeko1 cells. Mice were sacrificed according to institutional guidelines (signs of significant disease morbidity such as limb paralysis or greater than 20% weight loss). Animal experiments were approved and performed following the policies and regulations set forth by the Institutional Animal Care and Use Committee of Case Western Reserve University.

In combination experiments, statistical significances between groups were defined using the Mann-Whitney test followed by a two-stage step-up (Benjamini, Krieger, and Yekutieli) multiple comparisons, FDR=1%. The coefficient of drug interaction (CDI) [5] was used to assess the additive (CDI = 1), supra-additive (synergism, CDI < 1), or sub-additive (CDI > 1) effect of the treatment versus the control arms, as previously performed [6]. In single-treatment experiments, differences between tumor volumes were considered statistically significant using the Mann-Whitney test, $P<0.05$.

**References**

1. Johnson Z, Tarantelli C, Civanelli E, et al. IOA-244 is a Non-ATP-competitive, Highly Selective, Tolerable PI3K Delta Inhibitor That Targets Solid Tumors and Breaks Immune Tolerance. Cancer Res Commun. 2023;3(4):576-591.
2. Cappelli LV, Fiore D, Phillip JM, et al. Endothelial cell-leukemia interactions remodel drug responses, uncovering T-ALL vulnerabilities. Blood. 2023;141(5):503-518.
3. Tarantelli C, Gaudio E, Arribas AJ, et al. PQR309 Is a Novel Dual PI3K/mTOR Inhibitor with Preclinical Antitumor Activity in Lymphomas as a Single Agent and in Combination Therapy. Clin Cancer Res. 2018;24(1):120-129.
4. Ullman-Culleré MH, Foltz CJ. Body condition scoring: a rapid and accurate method for assessing health status in mice. Lab Anim Sci. 1999;49(3):319-323.
5. Wu J, Tracey L, Davidoff AM. Assessing interactions for fixed-dose drug combinations in tumor xenograft studies. J Biopharm Stat. 2012;22(3):535-543.
6. Jabeen A, Huang S, Hartley JA, Van Berkel PH, Zammarchi F. Combination of Camidanlumab Tesirine, a CD25-Targeted ADC, with Gemcitabine Elicits Synergistic Anti-Tumor Activity in Preclinical Tumor Models. Blood. 2020;136(Supplement 1):31-32.

## Supplementary Figure and Tables

### Supplementary Tables

**Table S1**. **Regions specifically sequenced by the probes in the targeted DNA-sequencing data.** Each row delineates the primary target of genomic spaces covered by the probes according to the Hg19 genome reference. [See excel file]

**Table S2. $IC_{50}$ values obtained in lymphoma cell lines after 96 hours of exposure to loncastuximab tesirine, SG3199 and isotype-control ADC (B12-C220-SG3249), in addition to CD19 surface protein expression in lymphoma cell lines as measured following an absolute fluorescence quantitation with Quantum Simply Cellular microspheres using rB4v1.2 antibody.** DLBCL, diffuse large B-cell lymphoma; ABC, activated B cell; GCB, germinal center B cell; MCL, mantle cell lymphoma; MZL, marginal zone lymphoma; CLL, chronic lymphocytic leukemia; PMBCL, primary mediastinal large B cell lymphoma; CTCL, cutaneous T cell lymphoma; ALCL, anaplastic large cell lymphoma; PTCL-NOS, peripheral T cell lymphoma-not otherwise specified; HL, Hodgkin lymphoma.

| HISTOLOGY | CELL LINE | LONCASTUXIMAB TESIRINE ($IC_{50}$, PM) | SG3199 ($IC_{50}$, PM) | RB4V1.2 NORMALIZED ANTIBODY BINDING CAPACITY | B12-C220-SG3249 ($IC_{50}$, PM) |
|---|---|---|---|---|---|
| ABC DLBCL | HBL-1 | 12.1 | 1.2 | 57597 | 2500 |
| ABC DLBCL | OCI-Ly-3 | 10 | 0.8 | 29163 | 1200 |
| ABC DLBCL | RCK8 | 35 | 1.2 | 88579 | 2500 |
| ABC DLBCL | RI-1 | 45 | 5.8 | 44683 | 3162.5 |
| ABC DLBCL | SU-DHL-2 | 400 | 1.1 | 10896 | 1300 |
| ABC DLBCL | TMD8 | 6 | 0.5 | 42808 | 550 |
| ABC DLBCL | U2932 | 1100 | 8.8 | 51776 | 5562.5 |
| GCB DLBCL | DB | 100 | 3.2 | 100060 | 300 |
| GCB DLBCL | DOHH2 | 0.5 | 0.5 | 15703 | 125 |
| GCB DLBCL | FARAGE | 2 | 0.9 | 132705 | 1650 |
| GCB DLBCL | KARPAS 422 | 31.1 | 5.3 | 147515 | 8000 |
| GCB DLBCL | OCI-Ly-1 | 1.4 | 1.4 | 17514 | 275 |
| GCB DLBCL | OCI-Ly-18 | 0.6 | 0.5 | 0 | 150 |
| GCB DLBCL | OCI-Ly-19 | 0.8 | 0.5 | 87842 | 175 |
| GCB DLBCL | OCI-Ly-7 | 1.4 | 1.1 | 68590 | 2250 |
| GCB DLBCL | OCI-Ly-8 | 0.3 | 0.5 | 58172 | 90 |
| GCB DLBCL | PFEIFFER | 790 | 14.6 | 77045 | 25000 |
| GCB DLBCL | SU-DHL-10 | 2.8 | 0.9 | 51975 | 750 |
| GCB DLBCL | SU-DHL-16 | 2812.5 | 1.1 | 25787 | 2500 |
| GCB DLBCL | SU-DHL-4 | 9.5 | 1.4 | 176138 | 2250 |
| GCB DLBCL | SU-DHL-5 | 2 | 0.8 | 56953 | 650 |
| GCB DLBCL | SU-DHL-6 | 6.3 | 14.6 | 63374 | 9500 |
| GCB DLBCL | SU-DHL-8 | 1.5 | 1.2 | 66635 | 2500 |
| GCB DLBCL | TOLEDO | 13 | 1.4 | 75346 | 2812.5 |
| GCB DLBCL | VAL | 0.4 | 0.5 | 74808 | 340 |
| GCB DLBCL | WSU-DLCL2 | 3 | 1.8 | 9848 | 1500 |

| | | | | | |
|---|---|---|---|---|---|
| PMBCL | KARPAS 1106P | 1.5 | 0.6 | 126819 | 690 |
| MCL | GRANTA519 | 1.4 | 0.5 | 50553 | 400 |
| MCL | JEKO1 | 5.3 | 0.5 | 45616 | 2250 |
| MCL | JVM2 | 5.5 | 2.0 | 47160 | 3000 |
| MCL | MAVER1 | 2.8 | 0.7 | 98854 | 900 |
| MCL | MINO | 1 | 0.5 | 115483 | 450 |
| MCL | REC1 | 20000 | 32.2 | 80734 | 32500 |
| MCL | SP49 | 1.3 | 0.5 | 40871 | 700 |
| MCL | SP53 | 2 | 0.5 | 72511 | 850 |
| MCL | UPN1 | 0.9 | 0.8 | 50600 | 600 |
| MCL | Z138 | 1.5 | 0.5 | 22049 | 300 |
| CLL | MEC1 | 5.5 | 0.5 | 92461 | 1800 |
| CLL | PCL-12 | 26 | 1.1 | 60314 | 2562.5 |
| MZL | ESKOL | 3 | 0.5 | 51311 | 650 |
| MZL | HAIR-M | 9.5 | 0.8 | 52925 | 900 |
| MZL | HC1 | 0.5 | 0.5 | 58951 | 200 |
| MZL | KARPAS 1718 | 0.7 | 0.5 | 36730 | 400 |
| MZL | SSK41 | 2 | 0.8 | 20233 | 650 |
| MZL | VL51 | 550 | 0.5 | 7497 | 450 |
| HL | AM-HLH | 600 | 0.8 | 0 | 300 |
| HL | KM-H2 | 2750 | 5.0 | 219 | 5250 |
| HL | L-428 | 14000 | 29.2 | 0 | 13750 |
| PTCL-NOS | FE-PD | 850 | 0.5 | 0 | 750 |
| ALCL | KARPAS 299 | 11500 | 17.5 | 0 | 12500 |
| ALCL | KI-JK | 4000 | 3.5 | 0 | 2962.5 |
| ALCL | L-82 | 5750 | 1.2 | 0 | 5500 |
| ALCL | SU-DHL-1 | 700 | 0.8 | 0 | 600 |
| CTCL | MAC1 | 900 | 0.5 | 0 | 1500 |
| CTCL | H9 | 1500 | 2.3 | 0 | 900 |
| CTCL | HH | 35000 | 23.4 | 0 | 24000 |
| CTCL | HUT-78 | 3500 | 0.8 | 0 | 1700 |
| Canine B cell lymphoma | CLBL1 | 175 | 0.5 | 0 | 175 |
| Murine B cell lymphoma | A20 | 2012.5 | 1.0 | 0 | 850 |
| Murine B cell lymphoma | BCL1 clone 5B1b | 500 | 0.5 | 0 | 435 |

**Table S3. $IC_{50}$ values obtained in DLBCL cell lines after 72 hours exposure to R-CHOP.**

| CELL LINE | R-CHOP (IC50 UG/ML) |
|---|---|
| **DB** | 0.0476 |
| DOHH2 | 0.0150 |
| FARAGE | 0.0009 |
| HBL-1 | 0.0748 |
| KARPAS 422 | 0.0573 |
| OCI-LY-1 | 0.0066 |
| OCI-LY-18 | 0.0529 |
| OCI-LY-19 | 0.0097 |
| OCI-LY-3 | 0.0123 |
| OCI-LY-7 | 0.0082 |
| OCI-LY-8 | 0.0006 |
| PFEIFFER | 0.1471 |
| RCK8 | 0.0431 |
| RI-1 | 0.8127 |
| SU-DHL-10 | 0.0007 |
| SU-DHL-16 | 0.1338 |
| SU-DHL-2 | 0.2383 |
| SU-DHL-4 | 0.0113 |
| SU-DHL-5 | 0.0134 |
| SU-DHL-6 | 0.0029 |
| SU-DHL-8 | 0.0569 |
| TMD8 | 0.0134 |
| TOLEDO | 0.0771 |
| U2932 | 0.1542 |
| VAL | 0.0003 |
| WSU-DLCL2 | 0.2056 |

**Table S4**. **Mutational analysis in B cell lymphoma cell lines.** Mapping based on the Hg19 genome reference. [See excel file]

**Supplementary figures**

**Figure S1. Distribution of $IC_{50}$ values of loncastuximab tesirine (ADCT-402) between B and T-cell lymphoma derived cell lines.** ****, P<0.0001 as determined by the Mann-Whitney test.

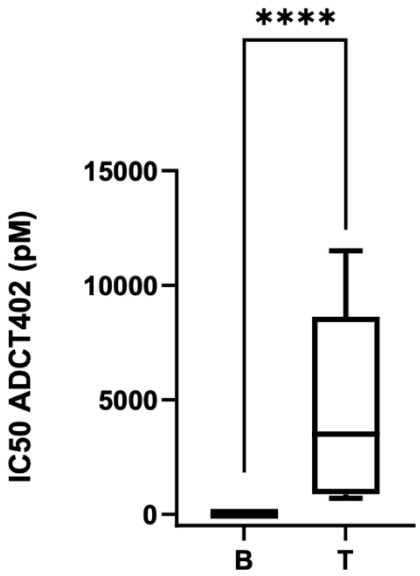


**Figure S2. Representative images of the apoptosis induction in two DLBCL cell lines exposed to loncastuximab tesirine (ADCT-402) and analyzed for annexin V by flow cytometry.** Cells were treated (2 x IC50) for 96 hours. The frequencies of annexin V positive cells (early apoptotic cells), annexin V/ propidium iodide double positive (late apoptosis), necrotic (annexin V negative, propidium iodide positive) and alive cells (annexin V/propidium iodide double negative) are shown.

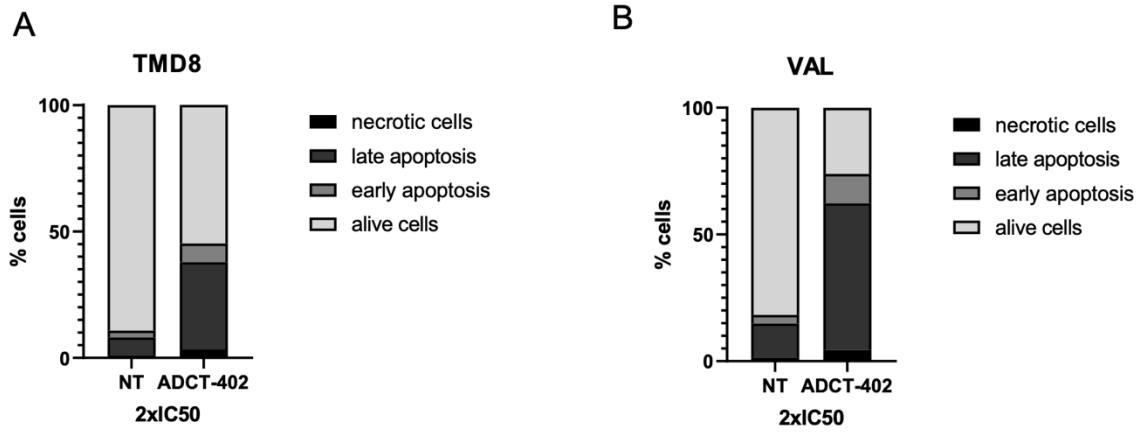

**Figure S3. Distribution of $IC_{50}$ values of loncastuximab tesirine among DLBCL cell lines based on the presence or absence of BCL2 and MYC chromosomal translocations as single or concomitant events (double hit) and of TP53 status.** A) DLBCL cell lines with (n=16) and without (n=7) *TP53* inactivation. B) DLBCL cell lines with (n=15) and without (n=11) *BCL2* translocation. C) DLBCL cell lines with (n=7) and without (n=19) concomitant *BCL2* and *MYC* translocation. D) DLBCL cell lines with (n=10) and without (n=16) *MYC* translocation. *, P< 0.05; **, P< 0.001.

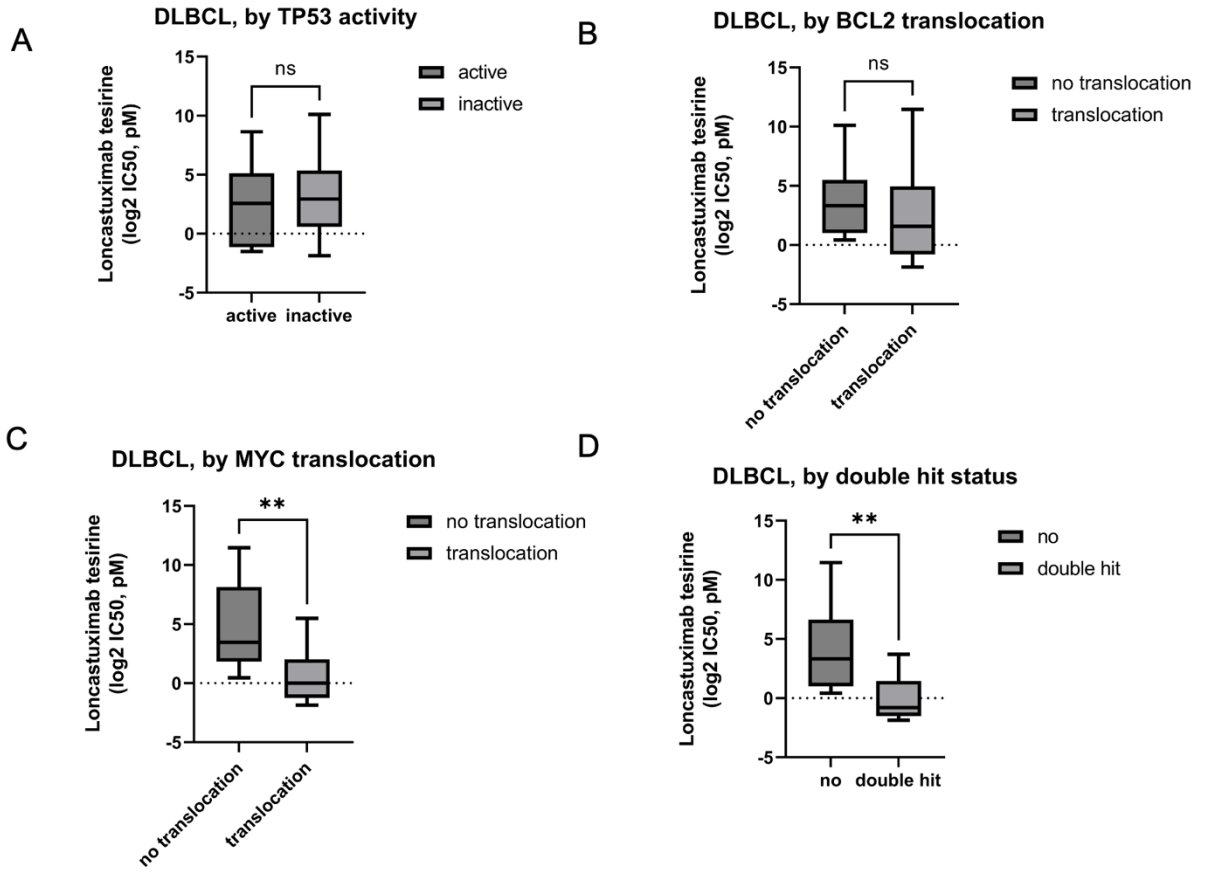

**Figure S4. MYC, CD19, and $IC_{50}$ values of loncastuximab tesirine among DLBCL cell lines.** A) CD19 surface expression between cell lines with and without MYC translocation. B) CD19 RNA expression values measured via RNA-Seq between cell lines with and without MYC translocation. C) CD19 RNA expression values measured via microarray between cell lines with and without MYC translocation. D) correlation plot between CD19 surface expression and MYC expression measured via RNA-Seq. E) correlation plot between CD19 RNA and MYC expression, both measured via RNA-Seq. F) Correlation between loncastuximab tesirine $IC_{50}$ values and MYC expression measured via RNA-Seq.

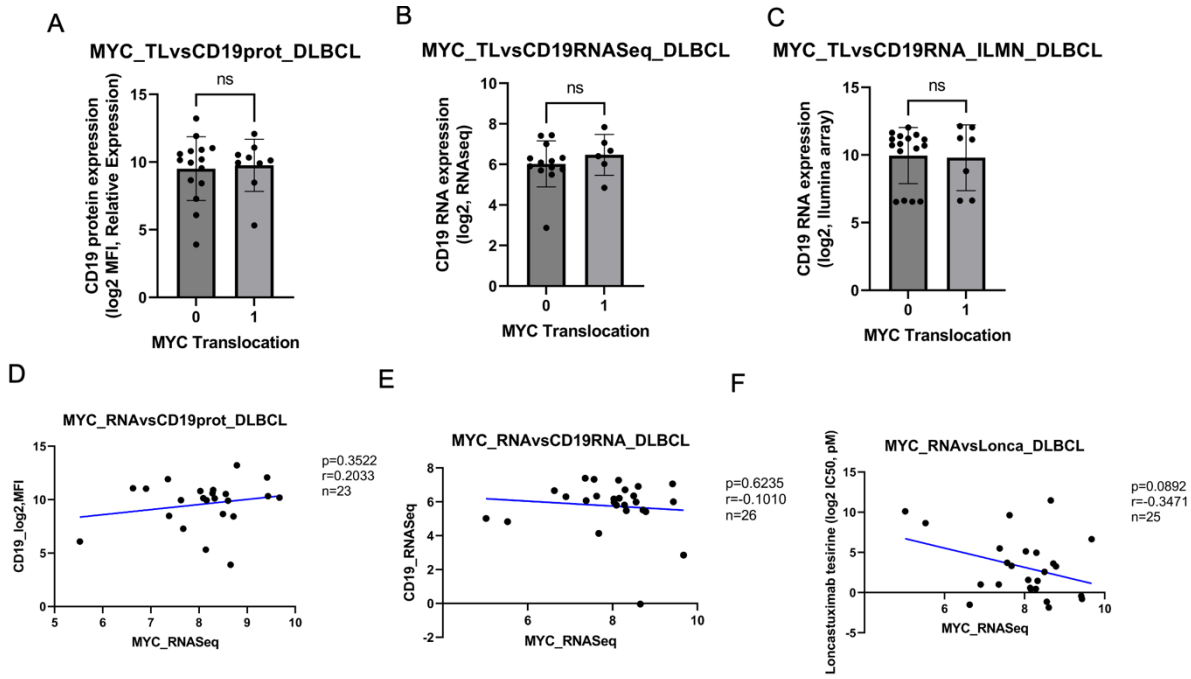


**Figure S5. Distribution of $IC_{50}$ values of SG3199 between B and T derived lymphoma cell lines.**

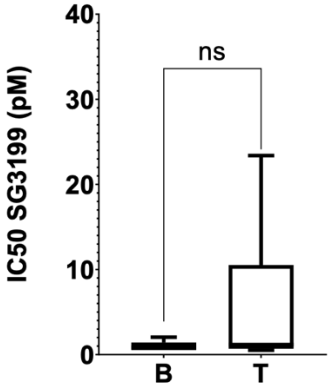

**Figure S6. Pearson correlation between SG3199 and CD19 absolute expression among B cell lymphoma cell lines.**

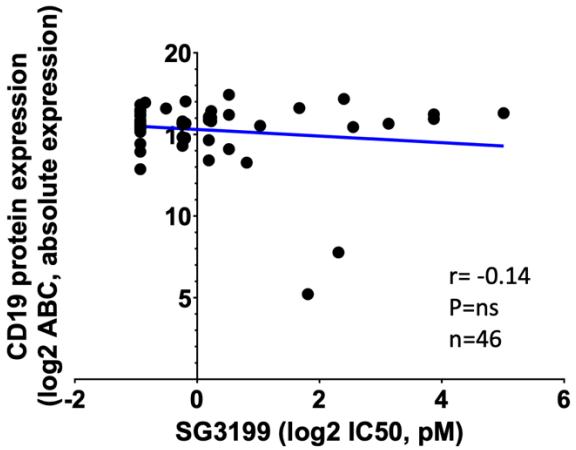


**Figure S7. Distribution of $IC_{50}$ values of loncastuximab tesirine and SG3199 across all cell lines (A) and among B cell lymphoma cell lines (B).** ****, P<0.0001 as determined by the Mann-Whitney test.

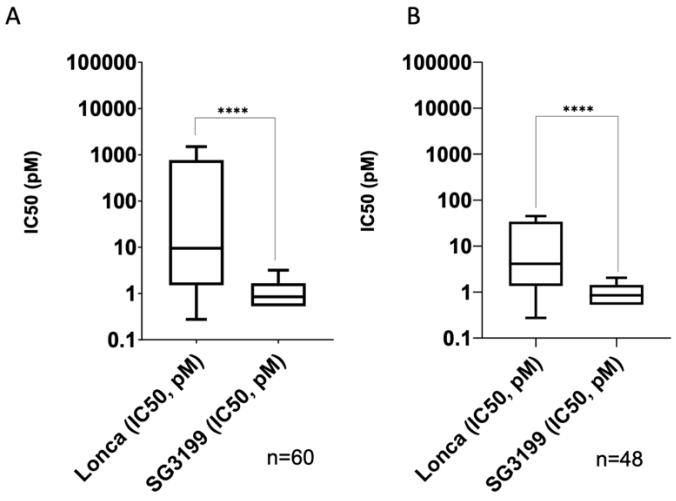

**Figure S8. Distribution of $IC_{50}$ values of SG3199 among DLBCL cell lines based on the presence or absence of BCL2 and MYC chromosomal translocations as single or concomitant events (double hit) and of TP53 status.** A) DLBCL cell lines with (n=16) and without (n=7) *TP53* inactivation. B) DLBCL cell lines with (n=15) and without (n=11) *BCL2* translocation. C) DLBCL cell lines with (n=7) and without (n=19) concomitant *BCL2* and *MYC* translocation. D) DLBCL cell lines with (n=10) and without (n=16) *MYC* translocation. *, P< 0.05; **, P< 0.001.

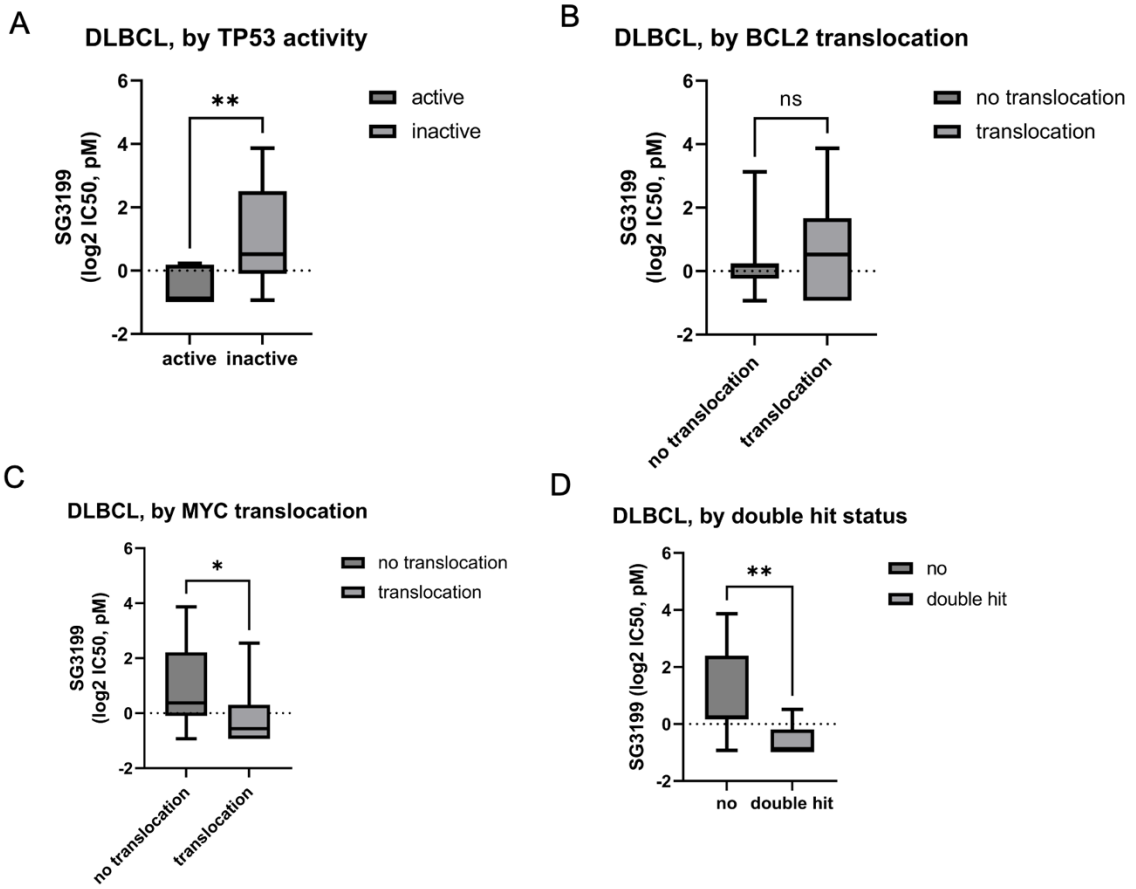

**Figure S9. Pearson correlation between SG3199 $IC_{50}$ values and MYC RNA levels measured via RNA-Seq (A) and via microarray (B) among DLBCL cell lines.**

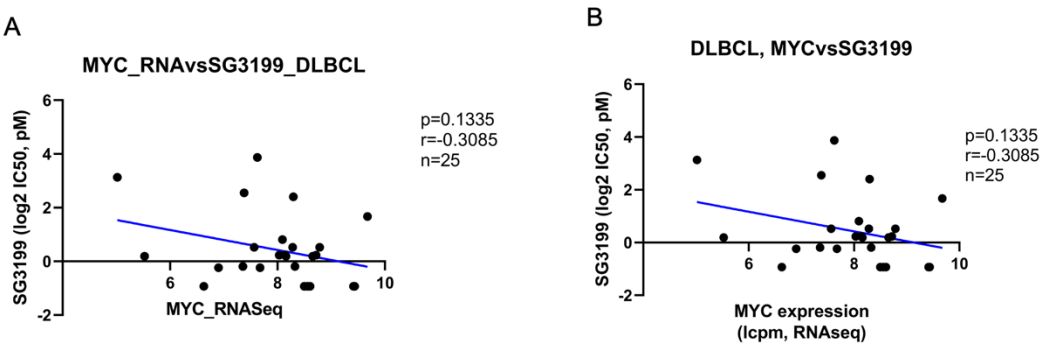


**Figure S10. SU-DHL-6 cell line is sensitive to loncastuximab tesirine and to its naked antibody, but it is resistant to its warhead SG3199.** Loncastuximab tesirine, SG3199, and rB4v1.2 activity was evaluated by MTT assay for 96 hours of treatment. X axis, concentration in pM; Y axis, fold to untreated. * q values < 0.05 of loncastuximab tesirine vs all other treatments (SG3199, rB4v1.2) was determined by unpaired t-test followed by two-stage step-up (Benjamini, Krieger, and Yekutieli) multiple comparisons, FDR(q)=0.05.

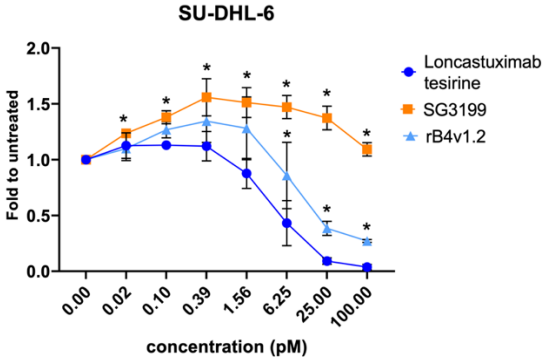


**Figure S11. Correlation between in vitro antiproliferative activities of loncastuximab tesirine and two others anti-CD19 ADCs.** Pearson correlations between log2 $IC_{50}$ (pM) of loncastuximab tesirine activity with coltuximab ravtansine (SAR34199) (A) or huB4-DGN462 (B).

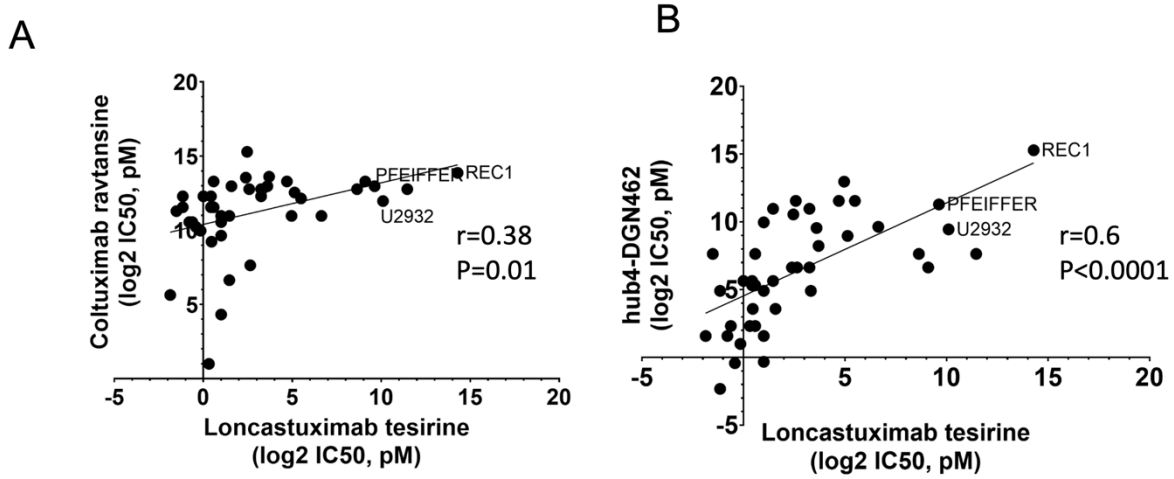

**Figure S12. Cell cycle distribution of DLBCL cell lines after 96h of treatment with loncastuximab tesirine alone or in combination with venetoclax, idelalisib or copanlisib.** TMD8 (A), WSU-DLCL2 (B), OCI-LY-3 (C) and VAL (D) were treated with two times $IC_{50}$. Statistics were calculated with the Student's t-test. *P value < .05. Single asterisk compares exposure conditions with the untreated sample.

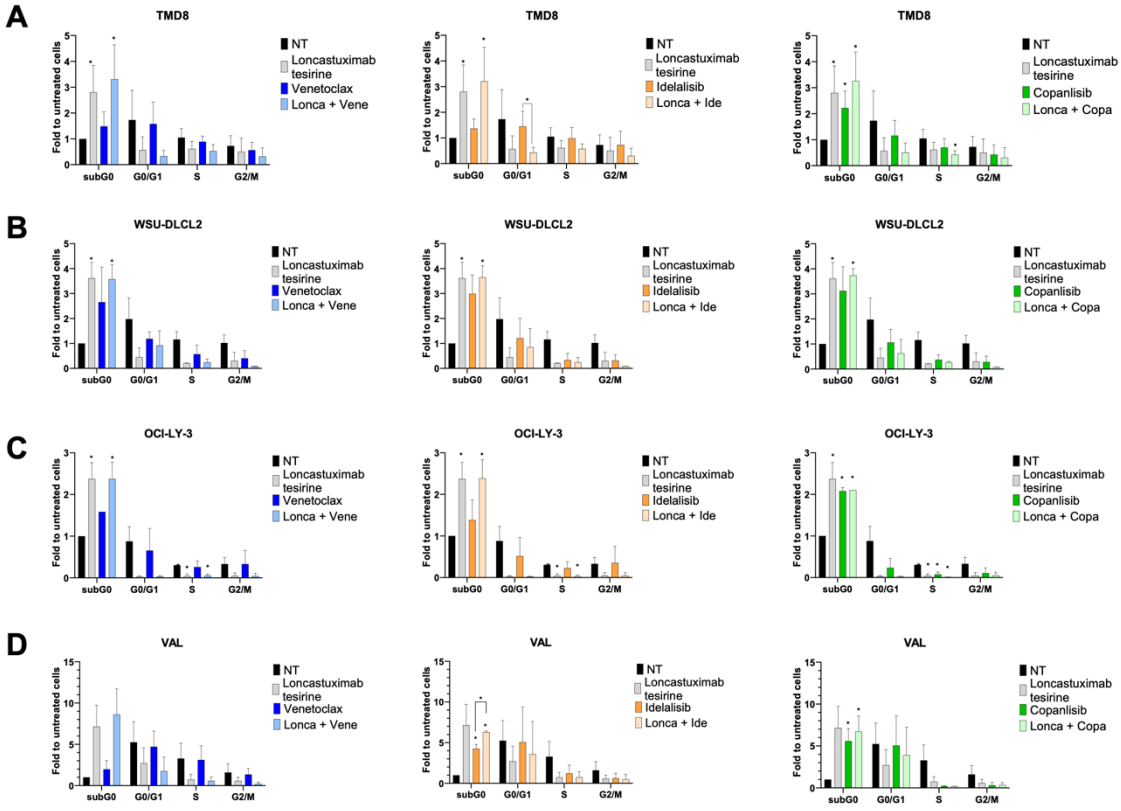

**Figure S13. Quantification of protein changes in cells treated with loncastuximab tesirine as a single agent or in combination with venetoclax, idelalisib, and copanlisib.**

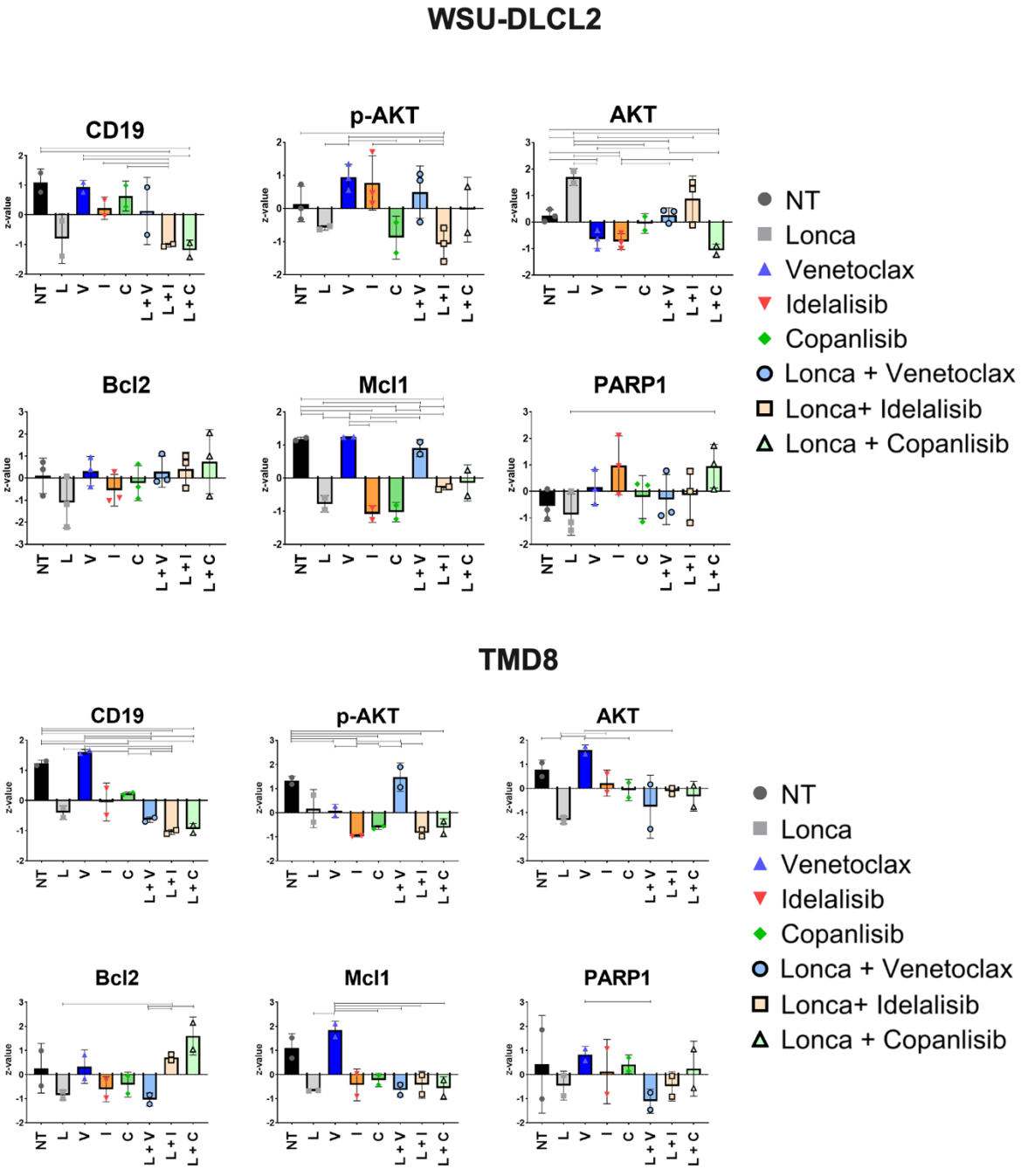

**Figure S14. PDX-derived lymphoma cells from one patient resistant to CD19 targeting CART cells are sensitive to loncastuximab tesirine. (A**) PDX-derived lymphoma cells from one patient resistant to CD19 targeting CART cells were left unstained and stained with anti-human-CD19-PE and isotype-PE, and then flow cytometry was performed. The number of events (count), median PE-value, and Frequency of PE-positive cells are shown in the figure. MTT results are shown in **B** and **C.** Cells were treated with the necked antibody rB4v1.2, the isotype associated with the toxin (B12-C220-SG3249), loncastuximab tesirine and the toxin SG3199 at increased doses for 96 hours.

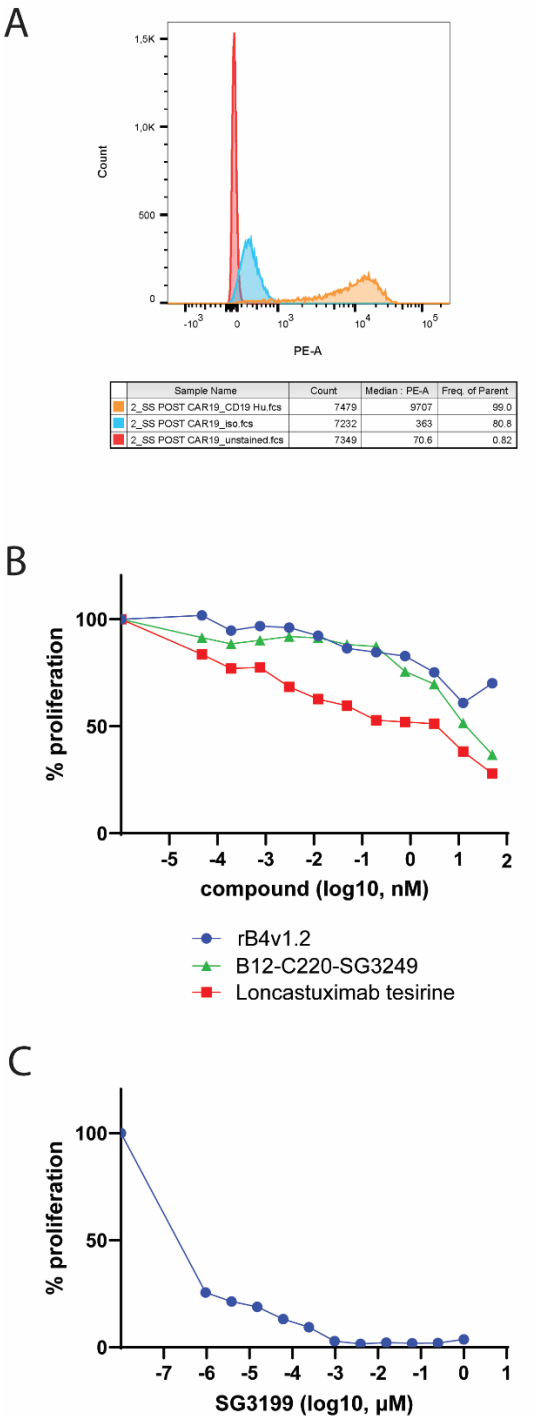


| Sample Name | Count | Median : PE-A | Freq. of Parent |
|---|---|---|---|
| 2_SS POST CAR19_CD19 Hu.fcs | 7479 | 9707 | 99.0 |
| 2_SS POST CAR19_iso.fcs | 7232 | 363 | 80.8 |
| 2_SS POST CAR19_unstained.fcs | 7349 | 70.6 | 0.82 |

**Figure S15. Single agent in vivo activity of loncastuximab tesirine and B12-SG3249 in TMD8 ABC DLBCL.**

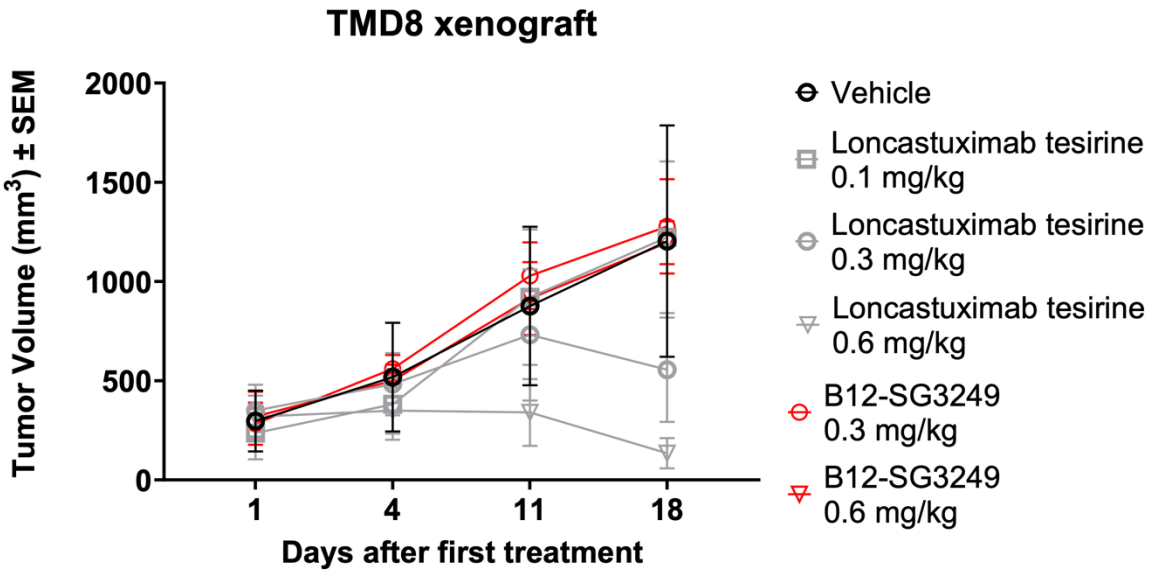


**Figure S16. Single agent in vivo activity of copanlisib in TMD8 ABC DLBCL.** * p values < 0.05 of copanlisib (both dosages) vs vehicle, as determined by Mann-Whitney test.

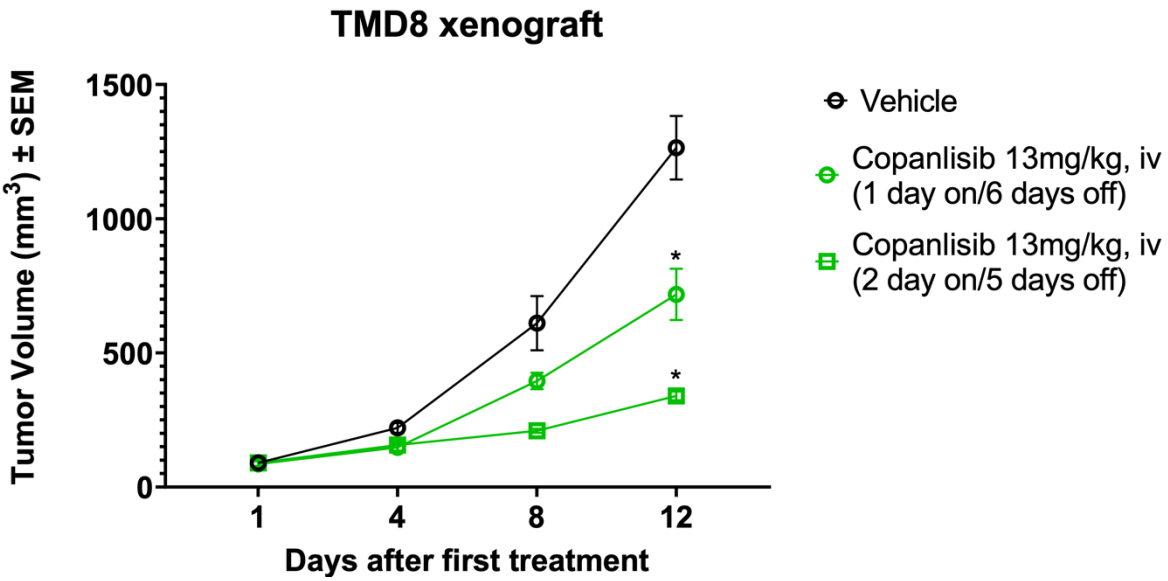

**Figure S17. Tumor weight in grams of xenografts from mice treated with loncastuximab tesirine in combination with copanlisib (TMD8) (A) or venetoclax (Jeko1) (B).** *, P<0.05; **, P<0.005; ***, P<0.0001 as determined by the Mann-Whitney test.